



HAL
open science

Anthropogenic climate change will intensify European explosive storms similar to Alex, Eunice, and Xynthia in the future

Mireia Ginesta, Emmanouil Flaounas, Pascal Yiou, Davide Faranda

► To cite this version:

Mireia Ginesta, Emmanouil Flaounas, Pascal Yiou, Davide Faranda. Anthropogenic climate change will intensify European explosive storms similar to Alex, Eunice, and Xynthia in the future. 2024. hal-04477289v1

HAL Id: hal-04477289

<https://hal.science/hal-04477289v1>

Preprint submitted on 26 Feb 2024 (v1), last revised 25 Jun 2024 (v2)

HAL is a multi-disciplinary open access archive for the deposit and dissemination of scientific research documents, whether they are published or not. The documents may come from teaching and research institutions in France or abroad, or from public or private research centers.

L'archive ouverte pluridisciplinaire **HAL**, est destinée au dépôt et à la diffusion de documents scientifiques de niveau recherche, publiés ou non, émanant des établissements d'enseignement et de recherche français ou étrangers, des laboratoires publics ou privés.

1 **Anthropogenic climate change will intensify European explosive storms**
2 **similar to Alex, Eunice, and Xynthia in the future**

3 Mireia Ginesta,^a Emmanouil Flaounas,^b Pascal Yiou,^a Davide Faranda,^{a,c,d}

4 ^a *Laboratoire des Sciences du Climat et de l'Environnement, UMR 8212 CEA-CNRS-UVSQ,*
5 *Univ. Paris-Saclay & IPSL, Orme des Merisiers, 91191 Gif-sur-Yvette, France*

6 ^b *Institute of Oceanography, Hellenic Center for Marine Research, Athens, Greece*

7 ^c *London Mathematical Laboratory, 8 Margravine Gardens, London, W6 8RH, UK*

8 ^d *LMD/IPSL, Ecole Normale Supérieure, PSL research University, 75005, Paris, France*

9 *Corresponding author: Mireia Ginesta, Mireia.Ginesta-Fernandez@lsce.ipsl.fr*

10 ABSTRACT: Extratropical storms, particularly explosive storms or 'weather bombs' with ex-
11 ceptionally high deepening rates, present substantial risks and are susceptible to climate change.
12 Individual storms may exhibit a complex and hardly detectable response to human-driven climate
13 change because of the atmosphere's chaotic nature and variability at regional level. It is thus essen-
14 tial to understand changes in specific storms for building local resilience and advancing our overall
15 comprehension of storm trends. To address this challenge, this study performs future projections
16 for three specific explosive storms, each impacting different European locations: Alex (October
17 2020), Eunice (January 2022), and Xynthia (February 2010). Using a dataset of 105 members
18 from the Community Earth System Model version 1 (CESM1), we identify analogues —storms
19 with a similar development stage— in two periods: the present-day climate (1991-2001) and a
20 future climate scenario characterized by high anthropogenic greenhouse gas emissions (RCP8.5,
21 2091-2101).

22 We evaluate trends in the frequency of occurrence of the storms and intensity, as well as on climate
23 drivers of impacts and the underlying dynamics. For all storms, our analysis reveals an increase
24 in precipitation and wind speed in the analogues of the future climate, specially for the explosive
25 ones. These findings underscore the potential consequences of explosive storms modified by cli-
26 mate change and their subsequent impacts on various regions of Europe, offering evidence that can
27 be used to prepare and enhance adaptation processes.

28 SIGNIFICANCE STATEMENT: This study investigates the impact of climate change on ex-
29 plosive storms, or 'weather bombs,' and their potential consequences for European regions. We
30 project future scenarios of three specific storms, Alex, Eunice, and Xynthia, using a state-of-the-art
31 climate model. Our findings reveal a trend of increased precipitation and wind speed in these
32 storms, emphasizing the heightened risks associated with climate change. The significance lies
33 in understanding the local implications of explosive storms, aiding in the development of resilient
34 strategies and adaptation measures.

35 **1. Introduction**

36 Weather variability in the mid-latitudes is controlled by atmospheric wave activity, consisting
37 of propagating synoptic-scale cyclonic and anticyclonic circulation. Therein, extratropical storms
38 play a key role in affecting the wave guide and producing the majority of high impact weather
39 (Wallace and Hobbs 2006). They contribute substantially to total precipitation (Hawcroft et al.
40 2012) and are a source of wind energy (Liu et al. 2008; Rapella et al. 2023). Extratropical storms
41 can also exhibit extreme behaviour, being associated with strong precipitation and flooding events
42 (Hawcroft et al. 2018), strong and damaging winds (Roberts et al. 2014a), or a combination of
43 both (Owen et al. 2021). Given their potential to become meteorological hazards with significant
44 socio-economic impacts (e.g., Liberato 2014; Jansa et al. 2001), understanding the evolution of
45 their characteristics in a future climate is crucial.

46 Several studies have assessed the role of climate change in modifying the underlying dynamics of
47 extratropical storms (e.g. Lehmann et al. 2014; Priestley and Catto 2022). Changes in frequency,
48 position and intensity of the storm tracks, namely the preferred regions where storms travel
49 through, are primary driven by changes in the horizontal temperature gradient in both lower and
50 upper troposphere and in the vertical temperature profile (Catto et al. 2019). The Coupled Model
51 Intercomparison Project (CMIP) phases 3, 5, and 6 generally agree on the spatial signature of
52 the projected changes in storminess in the North Atlantic (Harvey et al. 2020). Specifically,
53 models project a decrease in storm activity during summer, particularly in the southern regions,
54 and produce a tripolar pattern in winter of an increase in storm activity in the British Isles and
55 a decrease in the Mediterranean and Norwegian seas (Zappa et al. 2013; Priestley et al. 2020).
56 Regarding extreme storms, the response consist of a decrease in frequency of occurrence in the North

57 Atlantic basin, with a weak and local increase over the British Isles and the North Sea in winter
58 (Zappa et al. 2013; Seiler and Zwiers 2016). Sources of uncertainty of climate projections stem
59 from difficulties of isolating internal variability from the forced signal (Deser et al. 2012), as well
60 scenario and model uncertainty (Hawkins and Sutton 2009; Sansom et al. 2013). In addition, low
61 confidence still persists due to opposing thermodynamic processes that alter baroclinicity (Shaw
62 et al. 2016), and challenges in resolving meso-scale and small scale features such as the diabatic
63 processes (Schemm 2023).

64 While examining general trends in storm behaviour provides a fundamental understanding of
65 the impacts of climate change, it is essential to recognize that specific storms may exhibit unique
66 characteristics. This stems from the fact that specific storms are influenced by a combination of
67 factors that may not be accurately captured in general trends, giving rise to a chaotic nature in
68 the atmosphere and non-linear interactions. In addition, different regions may experience unique
69 environmental conditions, such as local topography or oceanic currents, resulting in diverse storm
70 behaviours in different areas. Hence, our study aims to bridge this gap by zooming in on the
71 particular features of extreme storms in different regions. For this reason, we employ an approach
72 within the field of Extreme Event Attribution (EEA) (Trenberth et al. 2015; Jézéquel et al. 2018),
73 specifically designed to address these questions. This field allows us to delve into the domain
74 of weather science to understand the specific meteorological conditions contributing to the event
75 while simultaneously evaluating the role of climate change in shaping its occurrence and intensity
76 (Shepherd 2016). We use a recent EEA approach that involves finding similar events, called
77 *analogues*, in two different time periods and comparing their key variables (Faranda et al. 2022).
78 Some studies have adapted this methodology to be more targeted for extratropical storms (Ginesta
79 et al. 2022; Faranda et al. 2023).

80 In our study, we further adapt this EEA approach for the analysis of explosive storms. Explosive
81 storms are characterized by a strong deepening rate in a short time period, and can produce
82 widespread damage when they make landfall (Liberato et al. 2013; Fink et al. 2009). These storms
83 were identified by Sanders and Gyakum (1980) as storms with a "Normalized central Deepening
84 Rate" (NDR_c) greater than 1:

$$NDR_c = \frac{DR_{24h} \sin(60^\circ)}{24h \sin(\varphi)}, \quad (1)$$

85 where DR_{24h} is the pressure difference over 24 hours measured at the storm center and φ is
86 the latitude at its second time step. These storms, also known as "weather bombs", are mainly
87 formed in regions of enhanced baroclinicity (Roebber 1984). In the North Atlantic, they primarily
88 form during the boreal winter in the western part of the basin, where there is a strong horizontal
89 temperature gradient linked to the Gulf Stream and land-sea contrast, large moisture availability
90 and strong vertical wind shear (Reale et al. 2019; Brayshaw et al. 2009).

91 We focus on three explosive storms that hit different parts of Europe: Alex in October 2020,
92 Eunice in January 2022, and Xynthia in February 2010. Unlike many EEA studies that compare
93 the present climate with a pre-industrial climate (factual and counterfactual periods), our method
94 uses present and future climate projections with the Community Earth System Model version 1
95 (CESM1). Our study aims to:

- 96 1. Evaluate how well CESM1 simulates storms with development stages similar to the three
97 targeted storms.
- 98 2. Analyze future climate trends in the frequency of these storms and their deepening rates, con-
99 sidering the scenario with the highest greenhouse gases emissions, that is, the Representative
100 Concentration Pathway 8.5 (RCP8.5).
- 101 3. Examine changes in the hazard levels of these events, quantified by measuring precipitation
102 and wind speed.
- 103 4. Characterize the underlying dynamics contributing to these observed changes.

104 In the subsequent sections, we describe the data and methods used (Section 2), explore the
105 characteristics of the storms (Section 3), analyze occurrence trends and intensity of storms (Section
106 4), and assess changes in climate drivers and underlying dynamics (Section 5). The conclusions
107 of our study are presented in section 6.

108 **2. Datasets and methods**

109 *a. Datasets*

110 To address the above objectives, we use the Community Earth System Model version 1 (CESM1;
111 Hurrell et al. (2013)), which is a global coupled climate model with a horizontal resolution of

112 about 1 degree. The radiative forcing applied in all simulations is the historical forcing until
113 2005 and the Representative Concentration Pathway 8.5 (RCP8.5) forcing from the CMIP5 project
114 (Meinshausen et al. 2011) from 2005 onwards. We use a multimember initial condition ensemble
115 CESM-LE (CESM-LE; Kay et al. (2015)), consisting of a 35-member ensemble of simulations
116 from 1 January 1920 to 2100. To increase the number of members, two additional ensembles of
117 35 members each are performed. In both, 35 members are rerun from perturbations of $O(10^{-13})$
118 on the initial atmospheric temperature field of the first member of the CESM-LE, starting at 1980
119 and at 2081 (Röthlisberger et al. 2020). After a few years, due to the chaotic nature of the climate
120 system, the members are in distinct states of their internal variability, and thus they are considered
121 to be independent (Fischer et al. 2013). Hence, the experimental set-up of this study consists
122 of 1050 years of a *present* climate, from 1991 to 2000, and 1050 years of a *future* climate, from
123 2091 to 2100. The radiative forcing is assumed to be relatively constant in a 10-year period. Kay
124 et al. (2015) showed that the spread of the CESM-LE due to internal variability is comparable to
125 CMIP5. In contrast to many CMIP5 models, CESM does not depict a too zonally oriented North
126 Atlantic storm track (Dolores-Tesillos et al. 2022). According to Dolores-Tesillos et al. (2022), the
127 model is able to reproduce fairly well storm frequencies and lifetimes, and most of the biases are
128 associated to weak or short living storms. However, there is an underestimated number of storms
129 over the ocean. At smaller scales, the model is able to represent the properties and structure of
130 extratropical storms and their associated warm conveyor belts (Joos et al. 2023; Binder et al. 2023).
131 The deepening rates of the weak and medium-strong storms in the NH in winter are also well
132 captured by the model but there is an underestimation of the explosive ones (Binder et al. 2023).

133 In this study we also use ERA5 reanalysis data (Hersbach et al. 2020), covering the period from
134 1950 to 2020, as a validation of the CESM model performance. The ERA5 dataset has a horizontal
135 resolution of 31 km.

136 The variables used from both reanalysis and CESM model are 6-hourly sea level pressure, hourly
137 precipitation rate, and hourly wind speed at 10m. To better assess the drivers of the differences
138 seen in CESM present and future periods we further analyze the following 6-hourly variables:
139 equivalent potential temperature (θ_e) at 850hPa, horizontal gradient of θ_e ($\nabla\theta_e$) at 850hPa, and
140 low-level Eady Growth Rate (EGR) between 850hPa and 500hPa. EGR is computed as:

$$EGR = 0.31 \frac{f}{N} \sqrt{\frac{\delta(u,v)}{\delta z}} \quad (2)$$

141 where $f = 2\Omega \sin\phi$ is the Coriolis parameter, $N = \sqrt{\frac{9.81}{\theta} \frac{\delta\theta}{\delta z}}$ is the Brunt-Väisälä frequency, and
 142 $\sqrt{\frac{\delta(u,v)}{\delta z}}$ is the vertical wind shear. Ω is the angular velocity of the Earth ($7.29 \times 10^{-5} \text{ rad/s}$), ϕ
 143 latitude, u and v zonal and meridional wind speeds, θ potential temperature, and z geopotential
 144 height.

145 *b. Methods*

146 We use the method of analogues (Yiou 2014), which has already been applied to the study of
 147 extratropical storms (Ginesta et al. 2022; Faranda et al. 2023), to find similar storms to Alex,
 148 Eunice, and Xynthia. In the context of this study, an analogue is defined as a storm with a similar
 149 development stage or a comparable track during its evolution. The full tracks of storms Alex,
 150 Eunice, and Xynthia are shown in figure A1 in the Appendix. We define the development stage
 151 of the storms as the 24h period before reaching their mature stage (figure A1 of the Appendix
 152 from points 0 to 1). First, we identify and track all storms in each dataset (ERA5, CESM present,
 153 CESM future). We use a Lagrangian approach where storms centers are defined and tracked as
 154 local minima in the sea-level pressure field (Wernli and Schwerz 2006). We then select the storms
 155 that have the most similar development stages to the targeted storms based on our definition of
 156 analogue. For that, we apply a two-step process:

- 157 • We first select all storms in the database that have a minimum sea level pressure lower than
 158 1000 hPa and located within a circle of radius 300 km of the targeted storm center in its
 159 minimum sea level pressure point. This filter ensures that only storms in their mature stage
 160 are considered and that they have reached their minimum sea level pressure in the vicinity of
 161 the targeted storm's center region. We refer to these storms as *mature stage* storms, and the
 162 time when they reach their minimum sea level pressure is defined as *time 0*.
- 163 • We select the last five grid points of the development stage of the mature stage storms. As
 164 we use 6-hourly data, this corresponds to the tracks 24 hours before the time 0 dates. For
 165 each mature stage storm, we compute the averaged Euclidean distance between the track of
 166 the storm and the track of the targeted storm. We select the 20% mature stage storms with the

167 lowest Euclidean distance from the targeted storm. This corresponds to the 20% most similar
168 development stage tracks. We term these *analogues*. The decision to use 20% is a trade-off
169 between finding tracks that resemble those of the targeted storms and having a sufficiently large
170 sample size to draw meaningful statistical conclusions. We tested that altering the percentage
171 to 10%, 15%, or 25% does not significantly impact our findings. We also select the analogues
172 that undergo explosive cyclogenesis, that is, that have a NDR_c greater than 1 (Eq. 1). We
173 term these *explosive analogues*.

174 3. Storm characteristics

175 In this section we contextualize the three storms by highlighting their particular features. We
176 also provide an overview of the storms associated impacts as well on the meteorological drivers.

177 a. Storm Alex

178 Storm Alex occurred in early October 2020 and was an early storm of the winter season. Alex
179 produced a devastating flood in the Alps region in 24 hours. The mechanism driving the Alpine
180 floods generally consists of an upper-level trough of large amplitude slowly moving eastward
181 towards the western Mediterranean (Massacand et al. 1998). In addition, Davolio et al. (2022)
182 showed that Alex produced extreme rainfall as it was associated with an atmospheric river coming
183 from the North Atlantic.

184 Alex was named by Météo-France on 30 September 2020. The storm produced most of the
185 damage on the 2 October 2020, giving rise to what is known as a Mediterranean Episode (WMO
186 2020). The heavy precipitation associated with Alex in the Alps produced several record-breaking
187 events, as high as 630 mm in a day recorded in Sambughetto (European State of the Climate 2020).
188 This Mediterranean episode also resulted in hurricane-force winds, such as 186 km/h in Belle-Île
189 - Le Talut (Météo France 2020). The passage of the storm left at least 15 fatalities (European State
190 of the Climate 2020) and economic losses estimated at more than 2 and a half billion euros (Aon
191 2020).

192 The storm developed as a secondary cyclogenesis, that is, as a frontal-wave instability along of
193 a synoptic front of a pre-existing storm. It deepened rapidly, enhanced by high upper level potential
194 vorticity values. The pressure dropped more than 30 hPa in the first 24 hPa, and the NDR_c was

195 about 1.6 B. It made landfall early 2 October when it reached its minimum sea level pressure on its
196 core (around 970 hPa). On its southern flank, the strong pressure gradient favoured high quantities
197 of water vapour transport, and an atmospheric river was formed from the subtropical western North
198 Atlantic to the vicinity of the storm core (Davolio et al. 2022). Storm Alex remained over France
199 for a day, producing record-breaking heavy precipitation in the Mediterranean area in southern
200 France and Northern Italy (Météo France 2020). In an EEA study based on reanalysis data Ginesta
201 et al. (2022), the persistence of the storm, as well as the accumulated daily precipitation, increased
202 in the present climate when compared to the recent past climate.

203 *b. Storm Eunice*

204 Eunice was the second storm of a cluster of winter storms (Met Office 2022) that lasted between
205 the 16th – 20th of February 2022 and mainly affected western Europe. The atmospheric config-
206 uration that embedded the storm cluster was characterized by a strong polar vortex, linked with a
207 high-speed jet stream that favored the intensification of the storms. The first storm of the cluster
208 was storm Dudley, or storm Ylenia in Germany. Dudley, characterized by strong wind gusts and
209 the formation of several tornadoes, affected western and central Europe. It ended with 9 fatalities
210 and an estimated insured economic loss of 1–2 billion (RMS). Eunice, the second storm of the
211 cluster, was a Shapiro-Keyser type storm (Shapiro and Keyser 1990), often associated with explo-
212 sive cyclogenesis and the formation of sting jets (Clark and Gray 2018; Manning et al. 2022). The
213 third storm of the cluster was Storm Franklin, characterized by flooding and high winds. However,
214 storm Eunice was the most impactful of the three.

215 Storm Eunice was named on the 14th of February 2022 by the UK Met Office, who issued
216 red weather warnings due to extremely strong winds on the 17th of February. Storm Eunice,
217 also known as Storm Zeynep or Storm Nora in Germany and Denmark, respectively, was a major
218 impact winter storm that struck several European countries from the 17th to the 20th of February.
219 The storm left multiple injuries and at least 17 fatalities in Europe (NL Times 2022; Anadolu
220 Agency 2022; Deutsche Welle 2022; BBC 2022; RTL Info 2022; The Irish Times 2022). Eunice
221 produced widespread damage and an insured loss estimated by the RMS at 2.5–3.5 billion (RMS
222 2022). Hundreds of flights were cancelled, millions of people were temporarily without power,
223 and schools were closed.

224 Eunice formed from secondary cyclogenesis on February 17 in the North Atlantic. It deepened
225 and moved rapidly northeast into England, experiencing explosive cyclogenesis with a central
226 pressure drop of 30 hPa in 18 hours and an NDR of 1.6 B. On February 18 at around 6 am Eunice
227 made landfall in Ireland and then crossed the UK in 12 hours. It produced widely spread damaging
228 wind gusts in many coastal areas, especially in the south of the UK. A wind gust of 196 km/h was
229 recorded in The Needles, Isle of Wight, the strongest ever recorded in England. On February 18 at
230 around 6 pm the storm was located over the North Sea reaching a sea level pressure in its core below
231 970 hPa, the minimum of its lifetime. In the hours that followed, the storm swept across Western
232 Europe with force, hitting in particular Germany, the Netherlands, and Belgium. On the February
233 19 at 6 am, Eunice was already located over the Baltic Sea, where it particularly affected Poland.
234 It then continued moving eastwards, weakening and dissipating as it crossed inland Northeastern
235 Europe.

236 *c. Storm Xynthia*

237 In winter 2009/2010, the general atmospheric circulation over Europe was characterized by an
238 extreme and record-persistent negative phase of the North-Atlantic Oscillation (NAO) (Cattiaux
239 et al. 2010). This led to a low position of the jet stream, several severe cold spells, cold weather
240 conditions and destructive storms. Xynthia was the strongest and most damaging extratropical storm
241 to hit Europe in winter 2009/2010. This extreme storm, which occurred in late February/early
242 March 2010, has raised interest in the scientific community due to its uncommon meteorological
243 characteristics (e.g. Liberato et al. 2013) and impacts (e.g. Chadenas et al. 2014; Vinet et al. 2012).

244 Along its lifetime, Xynthia followed an unusual SW-NE path passing over the western coast of the
245 European peninsula affecting mainly Portugal, Spain, France, Germany, Belgium and Denmark.
246 The storm caused more than 60 fatalities in Europe (García-Pereda (NWC SAF/AEMET) 2010;
247 Kolen et al. 2013). At least 53 of the deaths occurred in France (Chauveau et al. 2011), and 29
248 of those in La Faute-sur-Mer, a commune in the western coast, due to severe flooding (Genovese
249 and Przyluski 2013). The insured economic losses were estimated between 1.5 and 3 billion euros
250 (Worldwide 2010).

251 Xynthia began as a low-pressure system east of Bermuda on February 25, 2010, at around 30
252 degrees North in the subtropical Atlantic. Unlike most extratropical storms that intensify rapidly

253 when they cross the polar jet stream (Uccellini 1990), Xynthia’s intensification was primarily
254 driven by the advection of low-level warm, humid air and associated with high values of equivalent
255 potential temperature (θ_e) (Fink et al. 2012). The storm underwent explosive cyclogenesis between
256 the 26th and the 27th while rapidly approaching to the Iberian Peninsula, with a maximum NDR
257 of 1.9 B. On the 27th at 18:00 UTC it was already located west of the Bay of Biscay, reaching
258 its minimum sea level pressure below 970 hPa. It then swept across western France, resulting
259 in a powerful storm surge that locally exceeded 1.5 m and that produced most of the damages in
260 France (Bertin et al. 2012). Xynthia continued its path northeastwards hitting specially Belgium,
261 the Netherlands, Germany and Denmark. The storm dissipated around the 4 March over eastern
262 Scandinavia.

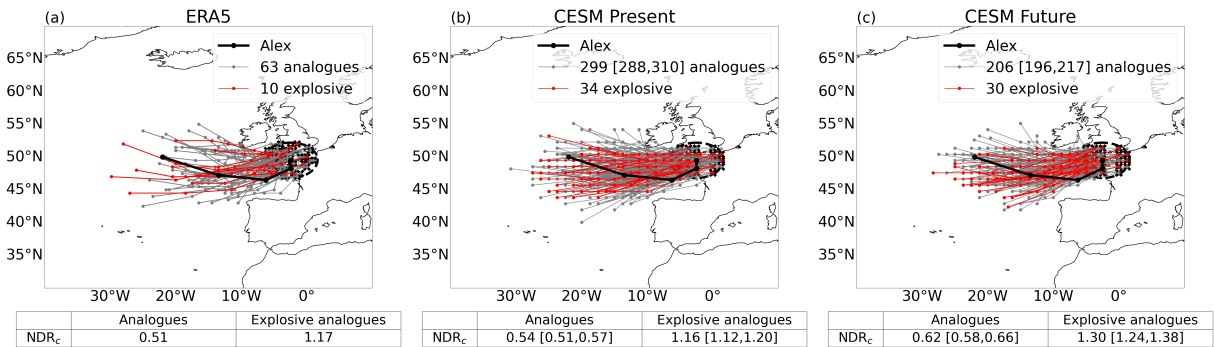
263 **4. Trends in frequency and intensity**

264 In this section, we first validate the CESM model performance in simulating analogue storms
265 of Alex, Eunice, and Xynthia, using ERA5 reanalysis data. Then, we assess future trends of
266 frequency of occurrence and intensity, measured by the NDR, by comparing CESM present and
267 future climates.

268 *a. Storm Alex*

269 Figure 1 shows the tracks during the development stage of the analogues and explosive analogues
270 of Alex for each dataset. The legends also display the number of analogues and explosive analogues.
271 In the ERA5 70-year period, 63 analogues have been identified, that is, around 9 analogues every
272 10 years. In contrast, fewer analogues are detected in the CESM present climate, with a frequency
273 of almost 3 analogues every 10 years. This could be due to an underestimation of storm frequencies
274 over the ocean (Dolores-Tesillos et al. 2022). In the ERA5 dataset, 10 of the 63 analogues are
275 explosive, corresponding to a relative frequency of around 16% of the analogues. Three of these
276 explosive analogues are known storms that made landfall in France (Table A1). The fraction of
277 analogues that are explosive in the CESM present period is slightly lower than that of ERA5 (34
278 explosive analogues out of 299 analogues, that is, around 11%). The NDR_c , used here as a measure
279 of the intensity, of the analogues and explosive analogues in CESM present is comparable to that
280 of ERA5. We further measure the similarity of the analogues to the storm by computing the mean

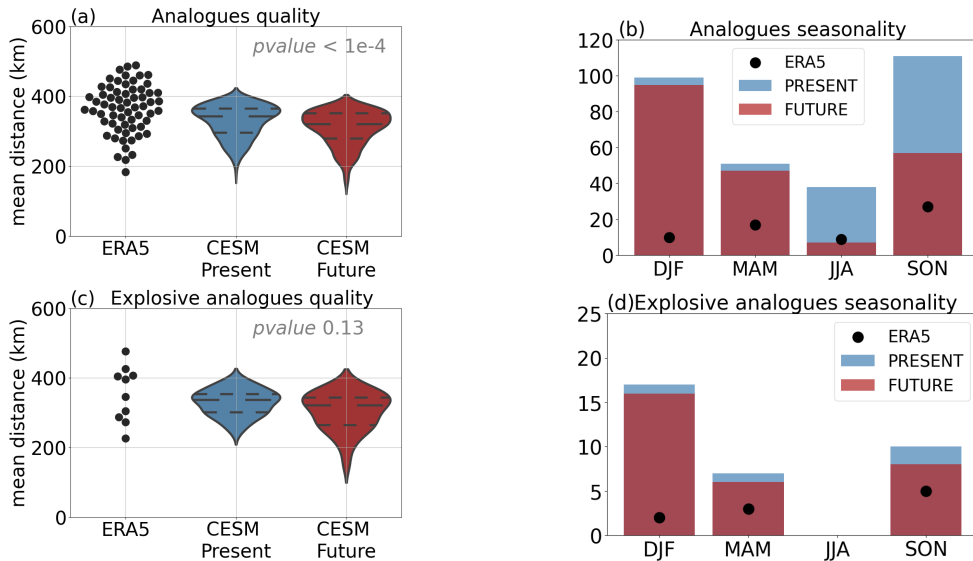
281 Euclidean distance between the 24-hour development stage tracks of the analogues and storm Alex.
 282 We term this *analogues quality* (Figs. 2a,c). The analogues quality distributions of CESM present
 283 show comparable values with ERA5, as no analogue was more than 500 km apart and most of them
 284 differed by around 380 km. These distributions indicate the model’s ability to simulate storms with
 285 development stage similar to Alex’s. Figures 2b,d show the number of analogues per season. Most
 286 of the analogues occur in autumn season in both ERA5 and CESM present. However, in ERA5 the
 287 second most preferred season is spring, while in CESM present is winter. Few analogues are also
 288 detected in summer in both, ERA5 and CESM present.



289 FIG. 1. 24-hour track of the development stage of storm Alex (thick black line) and its analogues (thin grey
 290 lines), for ERA5 (a), CESM present (b), and CESM future (c). Explosive analogues’ tracks are highlighted in
 291 red. The dashed-line circle indicates the 300-km area used to identify mature stage storms. The figure legend
 292 shows the number of analogues and explosive analogues. The tables beneath the figures depict the Normalized
 293 Deepening Rate values, calculated using equation 1, for both analogues and explosive analogues. 95 % confidence
 294 intervals for CESM present and CESM future, determined using a bootstrap test, are denoted in brackets.

295 There is a statistically significant decrease in the number of analogues in the future climate with
 296 respect to the present from 299 to 206 (Fig. 1). This decrease is mainly seen in autumn and
 297 summer, but there is also a slight decrease in winter and spring (Fig. 2b). There is little change
 298 in the number of explosive analogues (34 to 30) (Fig. 1), with a decrease in frequency mainly in
 299 autumn (Fig. 2d). However, the relative frequency of explosive storms increases from present to
 300 future periods from 11% to 15%. Additionally, there is an increase in NDR_c of both analogues
 301 and explosive analogues in the future climate with respect to the present, which is considered
 302 statistically significant because the confidence intervals do not overlap. This suggests that the
 303 analogues and explosive analogues in the future climate will be associated with more intense

304 deepening rates. Regarding the quality of the analogues, there is a statistically significant increase
 305 in the future period with respect to the present (Fig. 2a). This indicates that analogues in future
 306 conditions resemble better Alex’s development stage than in the present climate. In summary,
 307 anthropogenic radiative forcing is reducing the number of analogues of Alex, specially in autumn,
 308 but increasing their similarity to the storm as well as the deepening rates.



309 FIG. 2. (a,c) Mean Euclidean distances between the 24-hour track of the development stage of storm **Alex**
 310 and its **analogues** and explosive analogues for ERA5 (black dots), CESM present (blue probability distribution),
 311 and CESM future (red probability distribution). Dashed lines in violin plots show the quartiles 25%, 50%, and
 312 75%. A Kolmogorov-Smirnov test was used to determine the statistically significant difference between CESM
 313 present and future distributions, with the resulting p-value indicated in the figure. (b,d) Number of analogues per
 314 season: SON (September, October, November), DJF (December, January, February), JJA (June, July, August),
 315 and MAM (March, April, May).

316 *b. Storm Eunice*

317 In ERA5 we found 126 analogues, that is, around 18 every 10 years (Fig. 3). However, CESM
 318 again underestimates the number of analogues, detecting 6–7 every 10 years in the present climate
 319 (696). 23 out of 126 analogues are explosive in the ERA5 dataset, of which 8 are documented storms
 320 that had an impact in Europe (Table A1). This corresponds to a relative frequency of explosive
 321 storms of 18.3%. The relative frequency of analogues that undergo explosive cyclogenesis in

322 the CESM present is half of that of ERA5 (9.6%). In addition, the NDR_c of the analogues and
323 explosive analogues is slightly lower in the model than in ERA5 for both present analogues and
324 explosive analogues. Regarding the quality of the analogues (Fig. 4a), the analogues detected
325 by the model have lower mean Euclidean distances than those detected by ERA5. This indicates
326 that the model is good at reproducing storms that resemble Eunice's development stage. In the
327 ERA5 dataset, most of the analogues are found in autumn, while winter and summer have a similar
328 frequency (Fig. 4b). In the CESM present, the number of analogues in winter is slightly higher
329 than than in autumn.

330 Despite no significant changes in the number of analogues in the CESM future climate with
331 respect to the present climate (Fig. 3b,c), there is a decrease in frequency in autumn, summer and
332 spring, and an increase in winter (Fig. 4b). In the case of explosive storms, there is a significant
333 increase in the number of explosive analogues (67 to 95), corresponding to an increase in the
334 relative frequency of explosive cyclogenesis in a future climate. This increase is mainly seen in
335 winter (Fig. 4d), and a decrease again in autumn. The NDR_c of the analogues increases in a future
336 climate (Fig. 3b,c), but there are no significant changes in NDR_c of the explosive analogues. In
337 the future climate, the analogues and explosive analogues quality is better than in the present, as
338 evidenced by the statistically significant differences in probability distributions (Fig. 4a,c). As also
339 seen in Figure 3, the spatial spread in the development stage tracks of the analogues is lower in the
340 future climate, which means that future analogues represent Eunice's tracks better than those in
341 the present. In summary, there is a significant increase in the frequency of explosive cyclogenesis
342 in the future climate in winter. Additionally, the quality of analogues and explosive analogues
343 improves significantly in the future. These changes collectively suggest an increased likelihood of
344 Eunice-type storms in the future climate in winter.

345 *c. Storm Xynthia*

346 About 5 analogues every 10 years are detected in ERA5 and almost 1 every 10 years in the
347 CESM present dataset (Fig. 5). This suggests that the CESM model underestimates the number
348 of analogues that reach Galicia in their mature stage, linked to an underestimation of the storm
349 frequency in that region shown by Dolores-Tesillos et al. (2022). In terms of explosive occurrence,
350 3 out of 38 analogues underwent explosive cyclogenesis in ERA5 period, that is, around 8% of

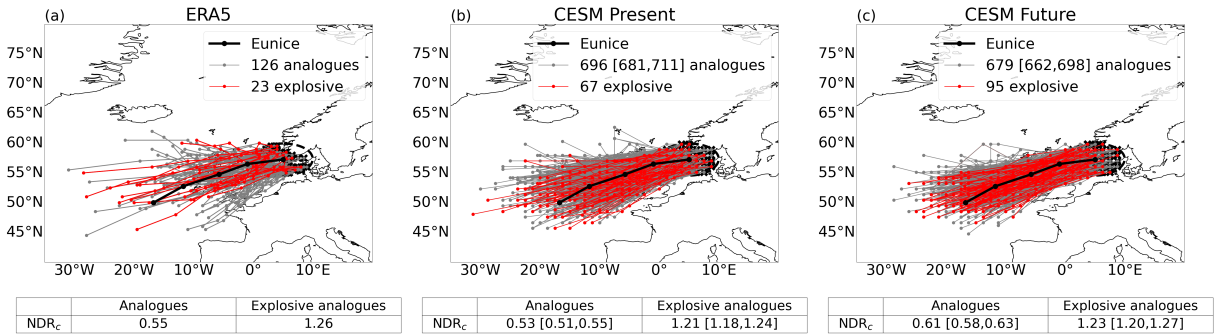


FIG. 3. Same as figure 1 but for storm **Eunice**.

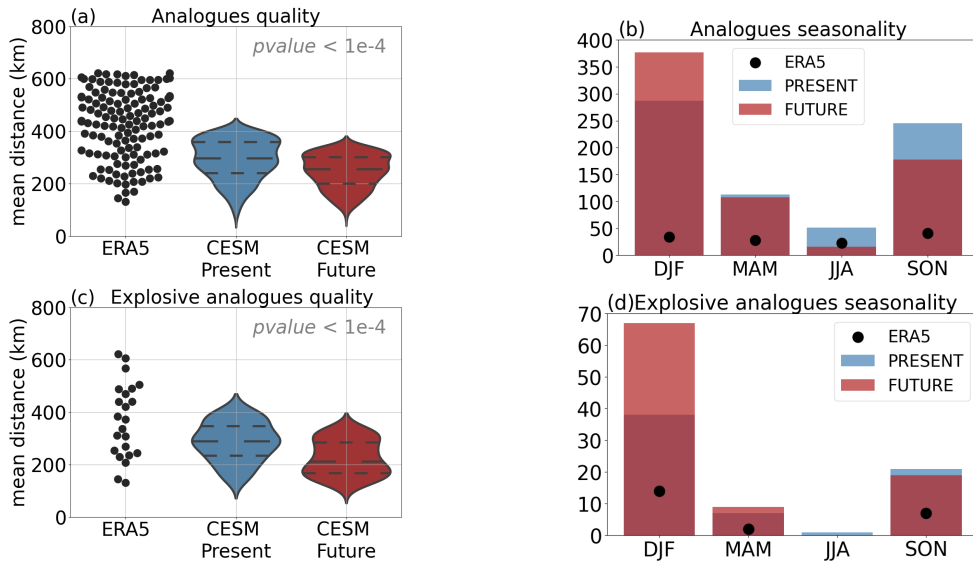


FIG. 4. Same as figure 2 but for storm **Eunice**.

351 the analogues. One of these is Miguel, a storm that affected western Europe in 2019 (Table A1).
 352 In the CESM present, the fraction of analogues that undergo explosive cyclogenesis is higher than
 353 in ERA5 (14 out of 101, that is, around 14%). In addition, the NDR_c of the analogues of the
 354 CESM present is higher than in ERA5. Despite the possible model biases, figures 6a,c show that
 355 the analogues and explosive analogues quality of the CESM dataset is comparable to that of the
 356 ERA5 period. In ERA5 the analogues occur more often in autumn, while in the CESM present
 357 dataset it is in spring (Fig. 6b).

358 In terms of the relative change between present and future climates, there is a significant decrease
 359 in the number of analogues in the future climate (101 to 68) (Fig. 5b,c). This decrease occur
 360 specially in spring, but also in autumn and summer (Fig. 6b). The number of explosive storms

361 decreased slightly (from 14 to 11), with a decrease in spring and autumn but an increase in winter
 362 (Fig. 6d). Hence, there is an increase in the relative frequency of explosive storms, from around
 363 14% to 16%. The NDR of the explosive analogues increases significantly under future climate
 364 conditions. However, due to the overlap in the confidence intervals, it is not possible to conclude
 365 that this increase is statistically significant, likely due to the insufficient sample size. No statistically
 366 significant changes are found in the analogues quality distributions between the two periods (Fig.
 367 6a,c).

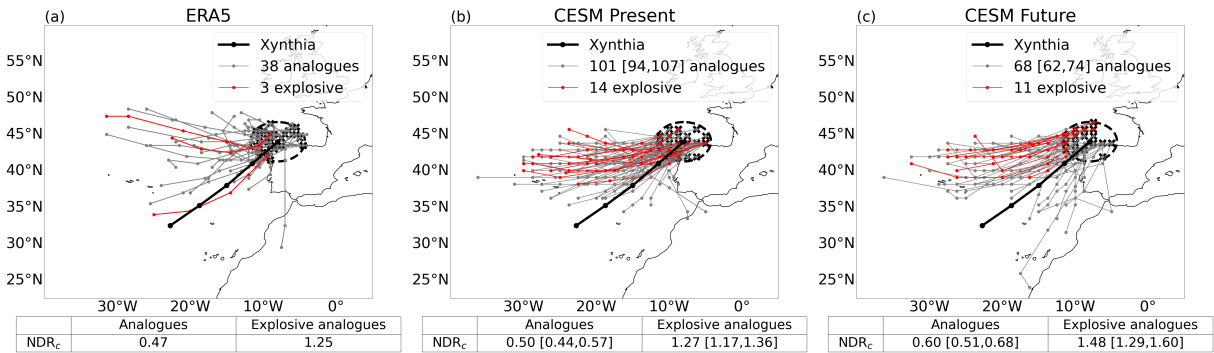


FIG. 5. Same as figure 1 but for storm Xynthia.

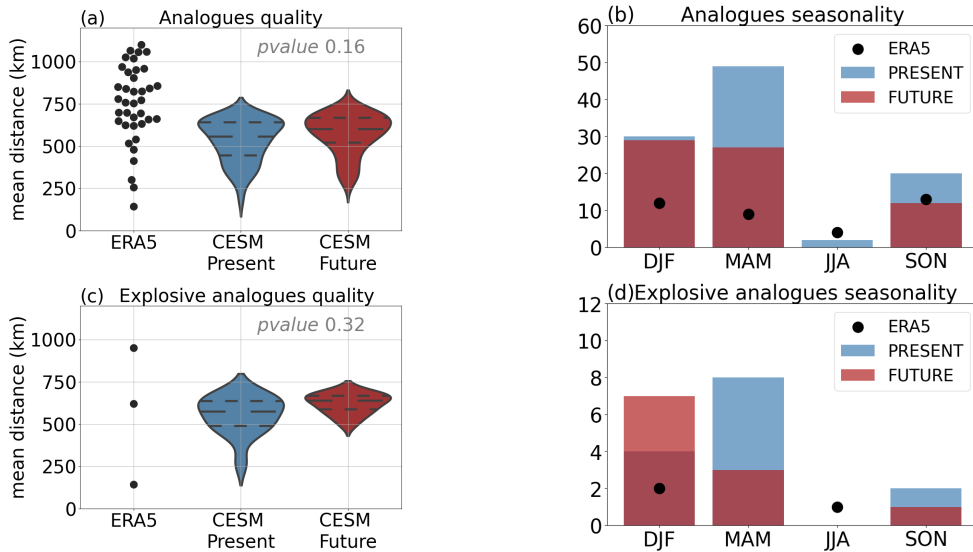


FIG. 6. Same as figure 2 but for storm Xynthia.

368 **5. Climate drivers of impacts**

369 In this section, we analyze trends in the fields of precipitation and wind speed at 10 m, commonly
370 known as key drivers of impacts. To gain deeper insights into the evolving patterns of explosive
371 analogues, we also assess the atmospheric dynamics contributing to these changes.

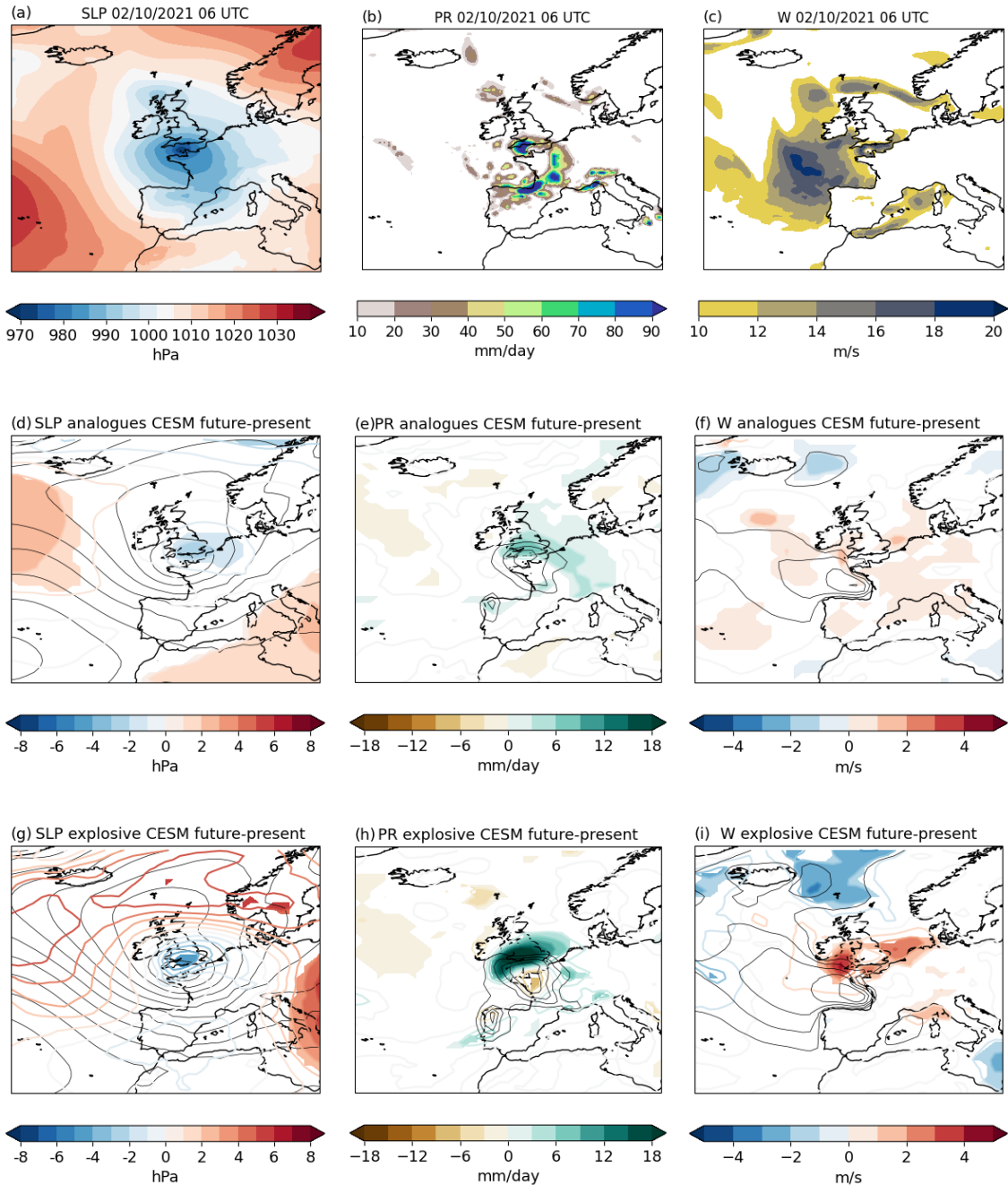
372 *a. Storm Alex*

373 Figures 7a,b,c show the sea-level pressure (SLP), precipitation rate (PR), and wind speed at 10
374 m (W) fields of storm Alex using ERA5 data at its time 0 date. The minimum SLP is around 970
375 hPa, and the storm center is squeezed over the English channel. Regarding PR, precipitation is
376 primarily located along the storm's frontal structure, as well as over the Southeastern France coast
377 and windward of the Alps. High wind speeds are predominantly observed in the southwestern
378 section of the storm. The CESM present composites of analogues and explosive analogues for
379 SLP, PR and W are shown in black contours in figures 7d–i as well as in figure A2 in the Appendix.
380 As expected, the pressure gradient in the explosive analogues composites is higher than that in
381 the analogues (higher and closer number of black contours in Fig. 7g,d, respectively), resulting
382 in lower SLP values in the storm core. In addition, explosive analogues are associated to higher
383 PR and W (black contours in Fig. 7h,i, respectively) than those of the analogues (Fig. 7e,f,
384 respectively). SLP composites of both CESM present analogues and explosive analogues (Fig.
385 7d,g) depict a cyclonic structure with the center over the English channel, consistent with Alex.
386 With respect to the PR pattern, this is predominantly located within the storm core and its southern
387 region (fig. 7e,h). Due to the lack of precise alignment of storm fronts among the analogues, the
388 PR pattern does not display a clearly defined frontal area. High values of W are located over the
389 southern flank of the storm and over sea (Fig. 7f,i).

390 Shading in figures (Fig. 7d–f) show differences CESM future – minus – present of the analogues
391 composites for sea-level pressure (SLP), precipitation rate (PR), and wind speed at 10 m (W),
392 respectively. The analogues in the future period show positive anomalies of SLP northward of the
393 Azores anticyclone as well as in the eastern Mediterranean (Fig. 7d). This contributes to increase
394 the amplitude of the Rossby waves. In addition, there are SLP negative anomalies in the core of
395 the analogues. This means that the analogues in the future period are associated to lower core
396 pressures and to an increased pressure gradient. This, in turn, contributes to increase W in the

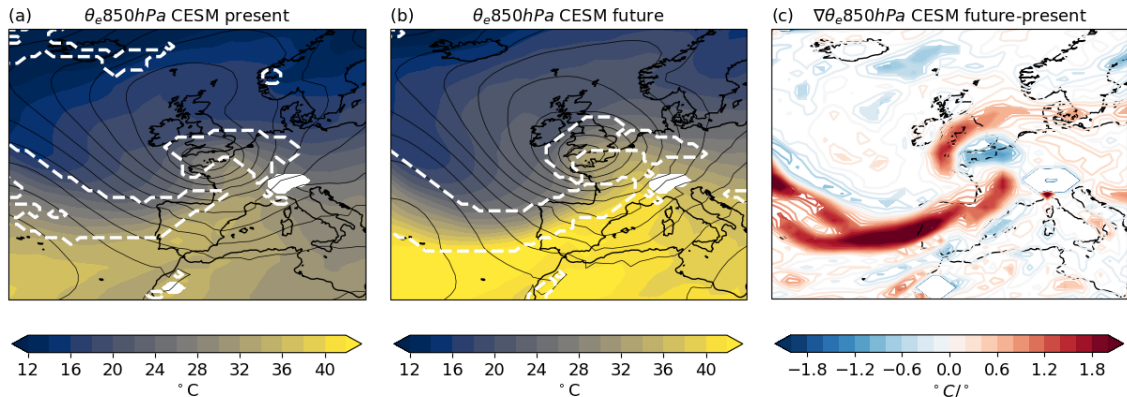
397 future period (Fig. 7f). In addition, PR increases, specially to the east of the storm core, in the
398 future period (Fig. 7e). The SLP differences of the explosive analogues depict a similar structure
399 to that of the analogues (Fig. 7g), with deeper storms in the future period and positive anomalies
400 on the eastern Mediterranean and southern Scandinavia. Hence, there is an increase in the SLP
401 gradient which is also reflected by an increase in W, specially to the east of the explosive analogues
402 core (Fig. 7i). Figure 7h depicts an increase of PR in the northern flank analogues' core and a
403 decrease, albeit smaller, southward.

404 The PR and W patterns of extratropical storms such as Alex and its analogues are mostly
405 influenced by the position and intensity of weather fronts. To assess changes in the weather fronts,
406 we evaluate the equivalent potential temperature at 850 hPa pattern (θ_e , figures 8a,b). We also
407 compute the gradient of the θ_e field ($\nabla\theta_e$). The regions of the maximum $\nabla\theta_e$ are shown by white
408 dashed lines in figures 8a,b, typically characterizing the presence of weather fronts. Figure 8c
409 illustrates the future minus present differences in $\nabla\theta_e$, providing insights into the changes in front
410 positions. In the CESM future, θ_e is overall higher than in the present, as a result of the expected
411 increase in global temperatures and water vapour content in a changing climate (shading in Fig.
412 8a,b). Regarding the regions of maximum $\nabla\theta_e$ (white dashed line in Fig. 8a,b), we interpret that a
413 cold front originates southwestern France and extends towards north of the Azores, as it is typically
414 characterized by cold temperatures behind the warm sector. The other regions of maximum $\nabla\theta_e$
415 are over English Channel extending towards central western Europe, and they would be associated
416 to the occluded and warm fronts, respectively. Regarding the future minus present differences
417 in $\nabla\theta_e$, we see a noticeable increase and a slight southward shift along the position of the cold
418 front (Fig. 8c). We also observe a northwestward shift in the warm front. These shifts lead to
419 a relocation of weather fronts of the explosive analogues in the future climate compared to the
420 present, potentially indicating a more rapid development of storms.



421 FIG. 7. (a) Sea level pressure (a), (b) precipitation rate, and (c) wind speed at 10 m for storm *Alex* at its time 0
 422 using ERA5 data. (d–i) Black contours: Composites of the Cesium present **analogues** and **explosive analogues**
 423 of storm **Alex** at their *time 0* dates of (d,g) sea-level pressure, at 4 hPa intervals, (e,h) hourly mean precipitation
 424 rate, from 10 mm/day and every 5 mm/day, and (f,i) hourly mean wind speed, from 10 m/s and every 2 m/s. Black
 425 contours are the same than shading in figure A2. Coloured contours: Cesium future minus present differences of
 426 the composites of the analogues. Shading: Cesium future minus present statistically significant differences.

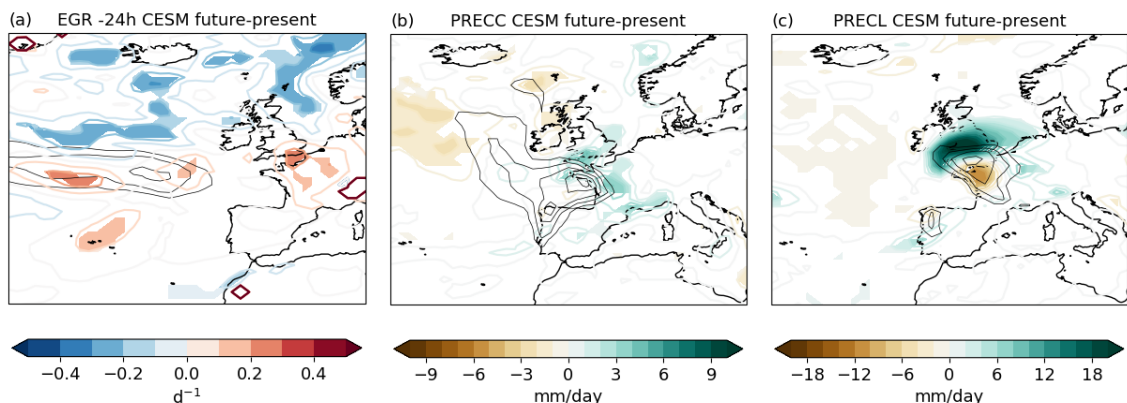
427 To further link changes in PR and W of explosive analogues with the dynamics and possible
 428 drivers, we assess the changes in eady growth rate (EGR, equation 2), convective precipitation
 429 (PRECC), and large-scale precipitation (PRECL). We observe a slight increase in EGR 24 hours
 430 prior to the mature stage of the storms, indicating an enhanced baroclinicity in future explosive
 431 analogues compared to the present (Fig. 9a). This could be linked to an increase in the NDR (Fig.
 432 1b,c) and in the intensity of storms in terms of wind speed (Fig. 7i). Furthermore, during the
 433 mature stage of the storms, we observe an overall increase in both PRECC and PRECL (Fig. 9b,c).
 434 Notably, PRECL contributes the most to the spatial changes observed in total precipitation (Fig.
 435 7h). These changes in the PRECL pattern might be linked with the cyclonic shift of the weather
 436 fronts seen in figure 8c and changes in the stratiform precipitation produced by the warm conveyor
 437 belt.



438 FIG. 8. (a,b) Shading: equivalent potential temperature at 850hPa for (a) CESM present and (b) CESM future
 439 **explosive analogues** of **Alex** at their time 0 dates. White dashed lines: values exceeding the 80th percentile of
 440 the equivalent potential temperature gradient at 850 hPa. Black contours: composites of SLP at 4 hPa intervals
 441 (same as the shading in figure A2). (c) CESM future minus present differences in the composites of the horizontal
 442 gradient of equivalent potential temperature at 850 hPa.

448 *b. Storm Eunice*

449 Storm Eunice was situated over the North Sea during its mature stage (Fig. 10a). At that time,
 450 precipitation was relatively modest along a frontal line (Fig. 10b), while wind speeds were notably
 451 high, especially over the sea on the southern flank of the storm (Fig. 10c). The composites of



443 FIG. 9. Shading: CESM future minus present differences in the composites of **explosive analogues** of (a) Eady
 444 growth rate 24 hours before the time 0 dates (EGR), (b) convective precipitation (PRECC), and (c) large-scale
 445 precipitation (PRECL), respectively. Black contours: composites of CESM present of EGR, PRECC and PRECL
 446 at intervals of $0.1 d^{-1}$ starting at $1 d^{-1}$, 2 mm/day starting at 5 mm/day, and 5 mm/day starting at 10 mm/day,
 447 respectively (same as shadings in Figures A3).

452 analogues and explosive analogues exhibit similar patterns of SLP, represented by black contours
 453 in figure 10d,g, respectively, and shading in figure A4a, d. In addition, the positions of highest PR
 454 and W in both analogues and explosive analogues (A4e,f and A4h,i) coincide with those of storm
 455 Eunice. Explosive analogues show, as expected, lower pressure at their core, and higher PR and
 456 W than the analogues.

457 The SLP pattern of the future analogues depicts lower pressures in the cyclonic structure and
 458 higher pressures in the anticyclonic with respect to the present analogues (Fig. 10d). This is linked
 459 to deeper analogues as well as an increase in the SLP gradient in their southern flank. The PR
 460 pattern depicts thus an increase in downstream of the analogues center and extended in western
 461 Europe (Fig. 10e). In terms of W, there is also an increase in the southern part of the analogues,
 462 that is, over the UK, the North Sea, and the Baltic Sea (Fig. 10f), which corresponds to the warm
 463 sector. The differences in the patterns of explosive analogues depict a similar pattern than the
 464 analogues: lower SLP, increase in PR, and stronger W specially over the sea (Fig. 10g,h,i).

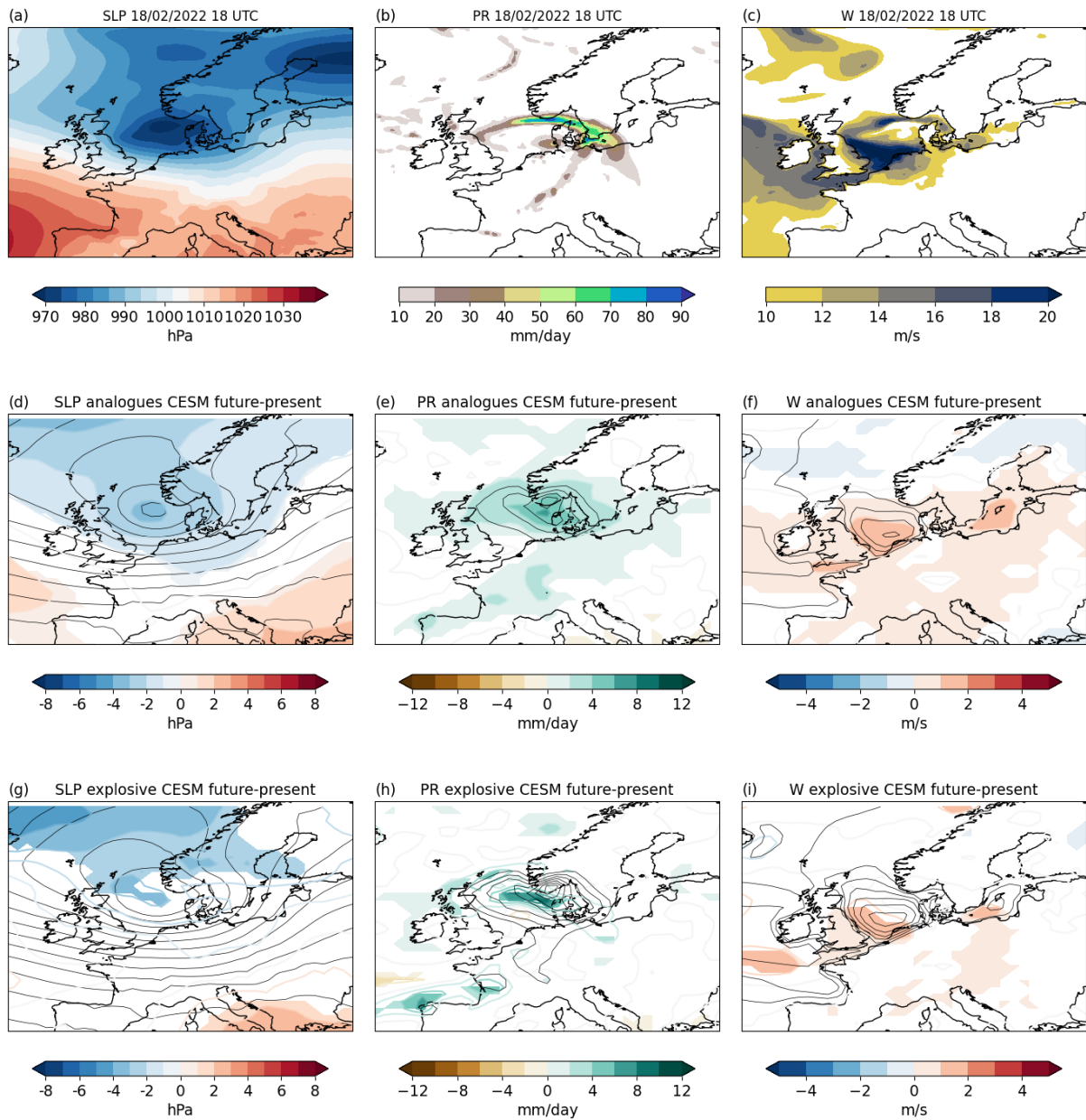


FIG. 10. Same than figure 7 but for **analogues of Eunice**.

465 Regarding the changes in $\nabla\theta_e$, figure 11c depicts an increase along a line starting in Germany
 466 and crossing central France and Bay of Biscay. This region corresponds to the southern flank of the
 467 cold front in the present climate, depicted in figure 11a in dashed white lines. Hence, the increase
 468 in $\nabla\theta_e$ can be interpreted as an intensification and a slight cyclonic shift of the cold front. This, in
 469 turn, might be linked to the increase in W in the cold sector seen in figure 10i and increase in PR
 470 over the cold front area (fig. 10h). On the contrary, a dipole pattern of $\nabla\theta_e$ over south Scandinavia
 471 suggests a deceleration of the warm front, shown in figure 11a as the tail of the comma-shape white
 472 dashed region.

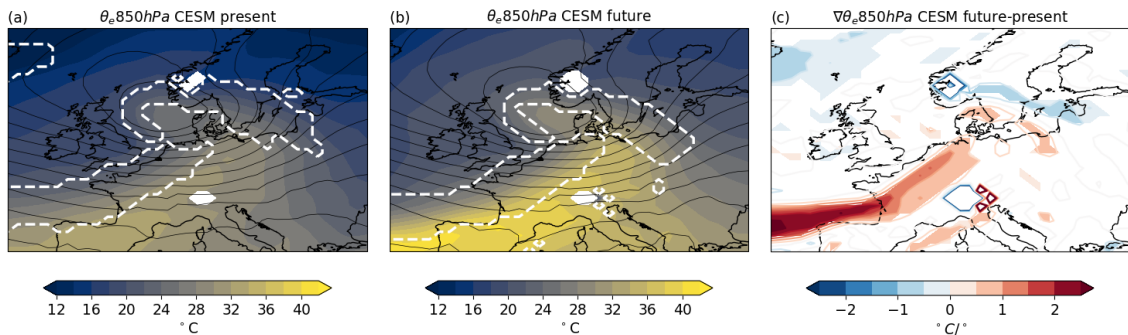


FIG. 11. Same as figure 8 but for storm **Eunice**

473 Figure 12a shows a significant increase in the EGR 24 hours before the time 0 dates of the
 474 explosive analogues in a future period. This suggests that the changes in intensity and patterns of
 475 the explosive analogues are largely baroclinically-driven. Little changes are seen in PRECC and
 476 (Fig. 12b), with an increase in the cold sector of the storm. Regarding the PRECL pattern, figure
 477 12c shows an increase over Bay of Biscay, probably linked to the increase in intensity of the cold
 478 front, as well as an increase over Denmark, where the warm front is located.

479 *c. Storm Xynthia*

480 The mature stage of storm Xynthia was situated over the Bay of Biscay (Fig. 13a). PR was
 481 primarily concentrated on the western flank of the storm (Fig. 13b), where the highest W was also
 482 observed (Fig. 13c). In this context, both analogues and explosive analogues successfully capture
 483 the mature stage's position (Fig. 13d,g). Regarding the patterns of PR and W (Fig. 13e,h and Fig.
 484 13f,i), both are slightly shifted southwards, probably due to a misalignment between the storm

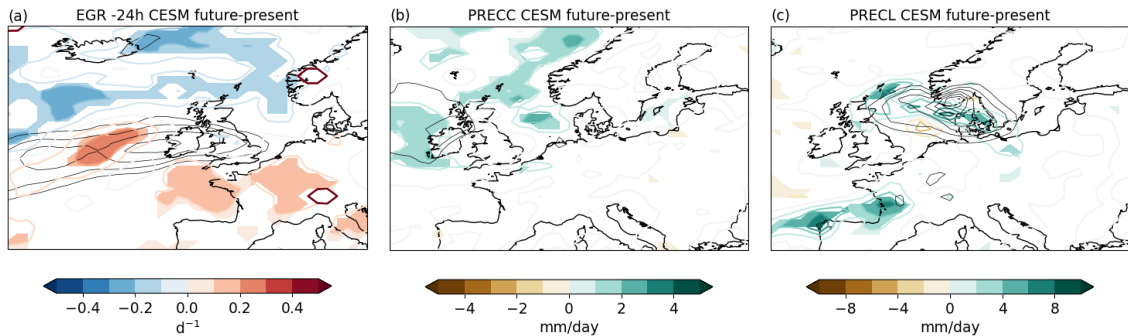


FIG. 12. Same as figure 9 but for storm **Eunice**

485 fronts. Similar to storms Alex and Eunice, explosive analogues demonstrate lower SLP and higher
 486 PR and W.

487 Figure 13d depicts lower pressures in the north part of the core of the analogues. In addition,
 488 there are positive anomalies of SLP in both western and eastern of the cyclonic structure, which
 489 results in an increase in the waviness of the pressure pattern. In the case of PR and W, both show an
 490 increase in the analogues core and northeastern of the Iberian Peninsula (Fig. 13e,f). Figure 13g
 491 shows that explosive analogues depict significant lower pressures in the future period, specially in
 492 their northern flank. This is linked with a significant increase in W (Fig. 13i). Similarly to Alex
 493 (Fig. 7h), PR depicts a significant increase in the northern flank of the explosive analogues' core,
 494 a slight decrease in the region of maximum PR in the present period, and a slight increase in their
 495 southern flank.

496 Figures 14a,b show a different spatial pattern of θ_e at 850hPa of present and future explosive
 497 analogues of Xynthia. In the present period, the warm sector of the storm does not overlap with
 498 the storm center. In contrast, in the future period the θ_e at 850hPa pattern has a T-bone structure,
 499 typical of the Shapiro–Keyser storms (Shapiro and Keyser 1990), and that could indicate a warm
 500 seclusion sector of the storms. In terms of changes in the gradient of θ_e , there is an overall increase
 501 of the gradient in the regions of the maximum gradient depicted by white dashed lines in 14a,b,
 502 which are the regions associated to the weather fronts. This is related to an increase in intensity of
 503 the weather fronts. A dipole with negative anomalies over the Bay of Biscay and positive anomalies
 504 northwestward suggest a cyclonic shift of the warm front position, even though the overall change
 505 is an increase in magnitude.

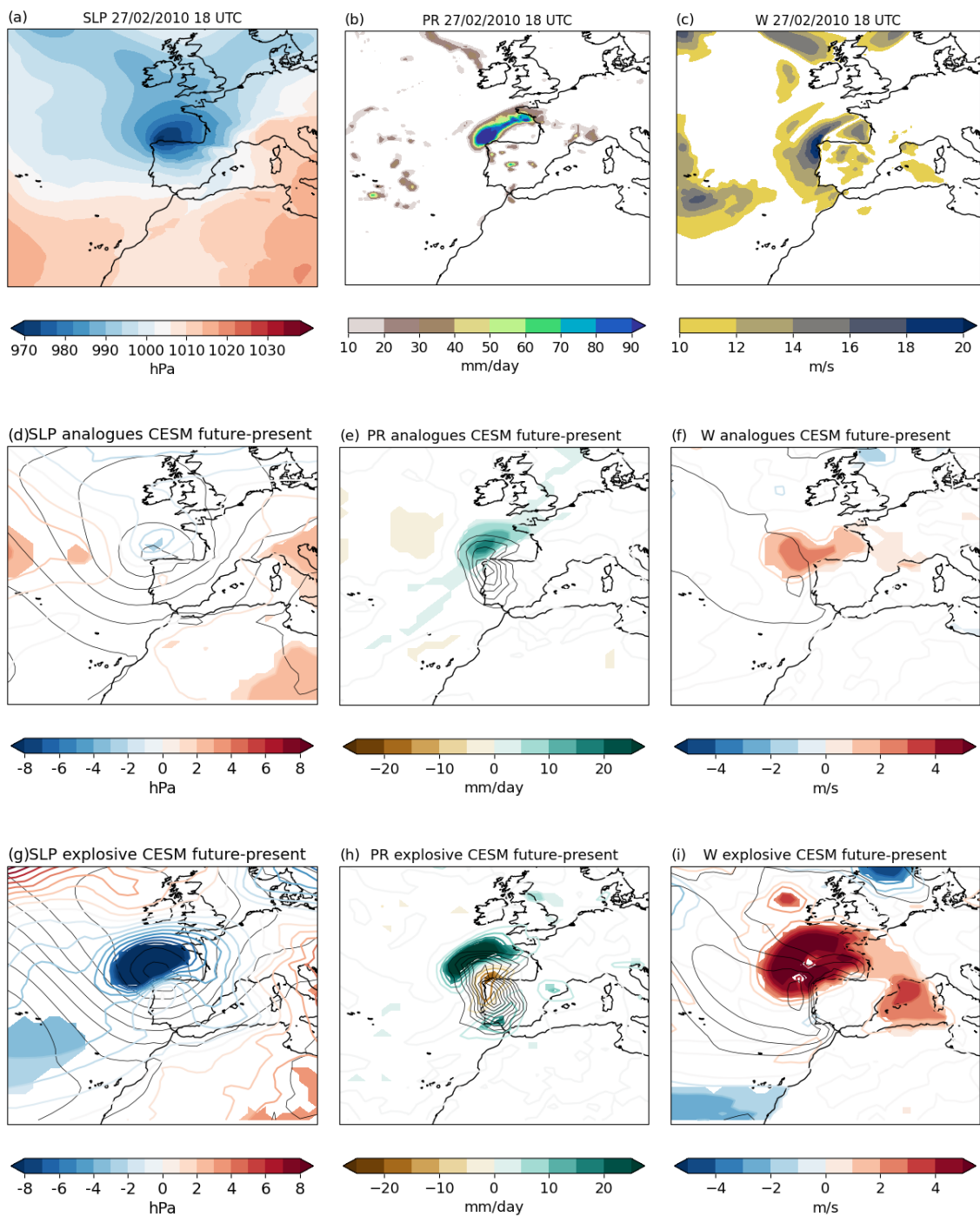


FIG. 13. Same as figure 7 but for **analogues of Xynthia**.

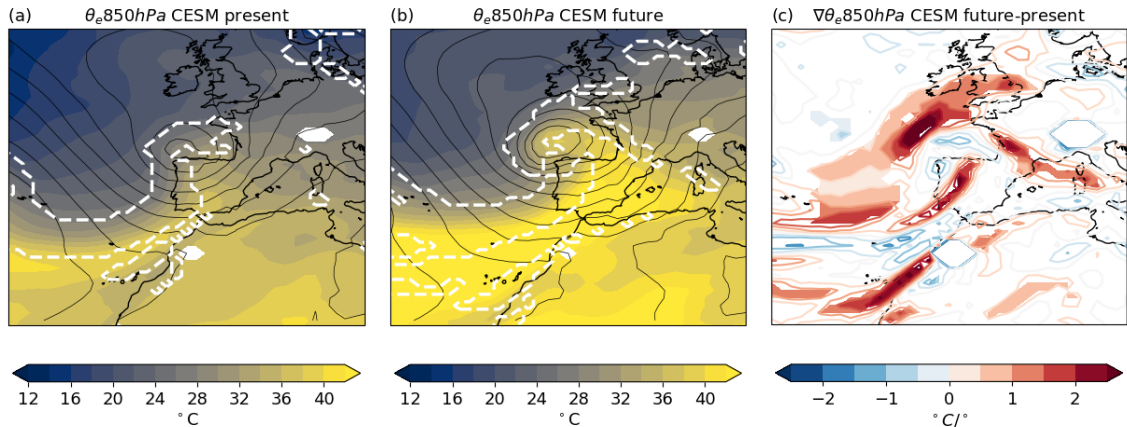


FIG. 14. Same as figure 8 but for storm **Xynthia**

506 Figure 15a depicts no change of the EGR in the region of its maximum, which means there
 507 are no changes in low-level baroclinicity. Thus, changes assessed previously might be completely
 508 diabatically-driven. Regarding PRECC and PRECL (Fig. 15b,c) spatial patterns, there is an overall
 509 increase in both types of precipitation. However, both show a tripolar pattern: a decrease in the
 510 core of the maximum precipitation area, and an increase in the southern and northern flanks. In
 511 the case of PRECL, this is linked to the cyclonic shift of the warm front and an intensification of
 512 both warm and cold fronts.

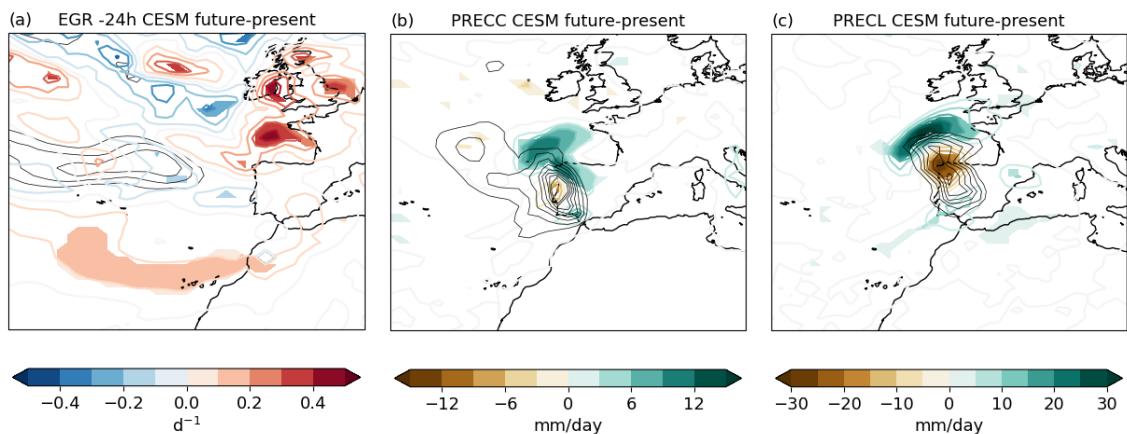


FIG. 15. Same than figure 9 but for storm **Xynthia**

513 **6. Discussion and conclusions**

514 We have conducted an analysis of three storms (Alex, Eunice, and Xynthia) under anthropogenic
515 radiative forcing, using the CESM-Large Ensemble. We identified storms with a similar devel-
516 opment stage to the three storms, and termed them *analogues*, in the present period (1991-2001)
517 and in the future RCP8.5 period (2091-2100). We further selected those undergoing explosive
518 cyclogenesis (*explosive analogues*). We found that the frequency and intensity of the analogue
519 storms, as well as their associated impacts, will change in a future climate.

520 For storm Alex, a significant decrease in the number analogues has been observed, specially in
521 autumn. However, there is an increase in the relative frequency of explosive analogues as well as
522 in the normalized deepening rates. Furthermore, both analogues and explosive analogues will be
523 associated with overall higher precipitation and stronger wind speeds. The large-scale precipitation
524 pattern of the explosive analogues and the weather front disposition suggest a cyclonic shift of the
525 mature stage of the storms. There is a small increase in the baroclinicity in the future explosive
526 analogues, which makes changes in their characteristics both baroclinically and diabatically driven.
527 These all suggest that explosive Alex-like storms will not be less frequent in a future climate, and
528 when they occur, they will deepen more rapidly and have larger impacts associated, indicating that
529 storms like Alex could be a greater meteorological hazard in the future.

530 For storm Eunice, rather than a change in the number of analogues, there is a seasonal shift
531 towards more analogues in winter and fewer elsewhere. However, we found a significant increase
532 in the number of analogues that undergo explosive cyclogenesis. The quality of both analogues
533 and explosive analogues also increases in a future climate. Additionally, there will be an increase
534 in precipitation rate and wind speed of the analogues and explosive analogues. These changes in
535 the characteristics of explosive analogues are, at least partially, baroclinically-driven. Therefore,
536 explosive Eunice-like storms will not only be more frequent but also more severe in a warmer
537 climate.

538 We found it difficult to identify good analogues of storm Xynthia in both reanalysis and climate
539 models. Hence, we can claim that storm Xynthia was an unusual event, and that a caveat of this
540 study is the quality of its analogues. We observed a decrease in the number of analogues, specially
541 in spring, but a slight increase in the relative frequency of explosive cyclogenesis. Xynthia-like
542 storms are expected to have higher precipitation rates and wind speeds in a future climate. The

543 explosive analogues depict an overall significant increase in precipitation and wind speed, with a
544 cyclonic shift in their mature stage. Changes in the patterns of explosive analogues are found to be
545 diabatically-driven. Therefore, Xynthia-like storms are becoming less probable but more severe,
546 especially those that are explosive, in a warmer climate.

547 Trends in the number of analogues, including explosive ones, depend on the specific storm
548 under consideration. Eunice-like explosive storms are expected to be more frequent, in line with
549 previous studies that project a slight increase in explosive frequency close to the British Isles and
550 on the North Sea (Seiler and Zwiers 2016; Zappa et al. 2013). The relative frequency of explosive
551 storms like Alex and Xynthia is also expected to increase with respect to the non explosive storms.
552 The increase in precipitation associated with storms in a future climate is consistent with other
553 studies (Hawcroft et al. 2018; Zhang and Colle 2017; Michaelis et al. 2017). For the explosive
554 analogues of Alex and Xynthia, we found a similar precipitation changes to Sinclair et al. (2020).
555 Sinclair et al. (2020) found, using aquaplanet simulations, a poleward displacement of the region of
556 maximum precipitation, mainly due to changes in the large-scale precipitation pattern, in a future
557 climate. There is less confidence in future projections regarding the dynamical intensity, such as
558 wind speed, associated to the storms (Seneviratne et al. 2021; Catto et al. 2019). However, our
559 study reveals that, across all the storms analysed, surface winds are expected to increase, specially
560 for the explosive analogues. For Eunice, the increase is located over the warm sector of the storms,
561 as consistent with previous studies (Priestley and Catto 2022; Dolores-Tesillos et al. 2022). The
562 drivers behind the changes in the pattern of the storms, whether they are baroclinically-driven or
563 diabatically-driven, vary depending on the storm. However, as found by Dolores-Tesillos et al.
564 (2022), Binder et al. (2023), and Joos et al. (2023), diabatic effects play a key role in increasing
565 the wind speed, the deepening rates, and the intensity of the strongest storms. For the case of
566 Xynthia, Ludwig et al. (2014) found that the storm intensification was mainly led by anomalously
567 high sea surface temperatures and diabatic processes, and also suggested that Xynthia-like storms
568 could be more frequent in a warmer climate. We note that we found no changes in baroclinicity
569 for Xynthia-like storms. Hence, we suggest that diabatic processes lead the increase in wind and
570 precipitation for Xynthia-like explosive storms in a future climate, as well as a relative increase
571 of the explosive frequency, consistent with the prediction by Ludwig et al. (2014). In addition
572 (Sinclair et al. 2020), found, using an aquaplanet model, that storms in a warmer climate are

573 more diabatically-driven. To better understand the potential influence of diabatic effects on storm
574 intensification, a comprehensive study on the role of warm conveyor belts in storm intensification
575 (Binder et al. 2023) could be conducted. Our study thus identifies both similarities and differences
576 when compared to previous research on various behaviors of extratropical and explosive storms
577 in the North Atlantic under climate change. These findings not only emphasize the differences in
578 regional trends but also suggest that storms may exhibit distinct behaviors compared to the overall
579 changes, potentially yielding different responses to anthropogenic radiative forcing.

580 Our approach has limitations that should be acknowledged. First, our analysis is based on a
581 single model, the CESM model version 1, which was chosen for its availability as a large ensemble
582 dataset of more than 100 members with 6-hourly data. While CESM has been shown to simulate
583 the characteristics of storms fairly well (Dolores-Tesillos et al. 2022; Joos et al. 2023; Binder et al.
584 2023) and to have a spread due to internal variability comparable to the CMIP5 multi-model spread
585 (Kay et al. 2015), a multi-model study would better assess model uncertainty. Second, we use a
586 single scenario, the worst-case scenario (RCP8.5), due to its availability. This scenario represents
587 an extreme case assuming high greenhouse gas emissions throughout the 21st century. Although
588 this extreme scenario proves valuable in detecting the anthropogenic radiative forcing signal, it
589 may not encompass the entire range of future climate projections. Therefore, our findings may not
590 be generalized to other scenarios. Future studies should explore the robustness of our results using
591 multiple models and scenarios. Finally, we use a single tracking scheme. However, we filter out
592 the weakest storms, and so the dependence on the tracking scheme is considered minor (Neu et al.
593 2013).

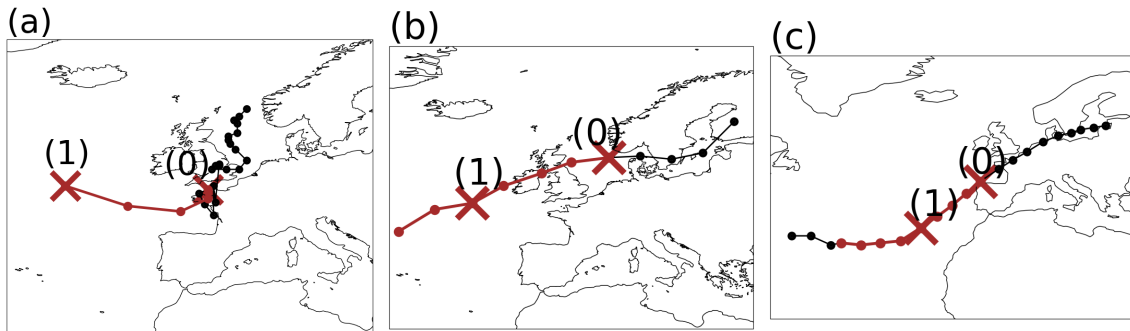
594 The analogues are considered recurrences in the atmospheric patterns of to the storms, and so
595 our results can also be applied to the explosive analogues found in the ERA5 dataset, some of them
596 being known high-impact storms in the region (Table A1). In conclusion, we found that all of
597 the storms analyzed in this study are expected to become more severe and impactful with climate
598 change. As suggested by Shepherd (2016), demonstrating that certain extreme events can occur
599 again and result in even worse consequences with climate change, as shown in this study, can help
600 advocate for investment in protective measures against hypothetical risks. Hence, these storms can
601 serve as reference points for building resilience and preparing for future events.

602 *Acknowledgments.* This work was supported by the European Union’s Horizon 2020 research and
603 innovation programme under the Marie Skłodowska-Curie grant agreement N° 956396 (European
604 weather extremes: drivers, predictability and impacts (EDIPI) ITN). The authors would like
605 to express special thanks to H. Wernli and his Atmospheric Dynamics group at ETH Zurich,
606 particularly M. Sprenger, M. Röthlisberger, H. Binder, J. Riboldi, and U. Beyerle, for their valuable
607 discussions and assistance in accessing the CESM data.

608 *Data availability statement.* The ERA5 data are publicly available online at
609 <https://cds.climate.copernicus.eu/>. We acknowledge the Atmospheric Dynamics and Climate
610 Physics groups at ETH Zurich for providing access to CESM data.

611

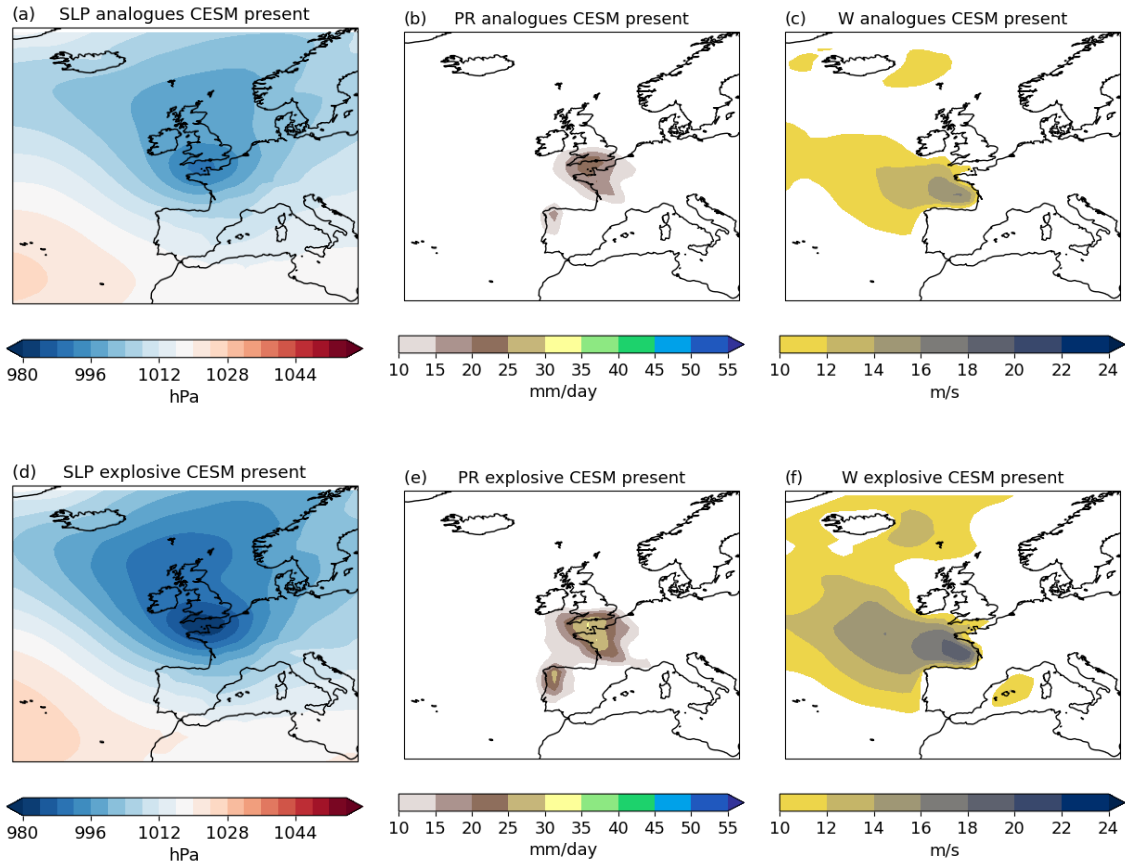
APPENDIX



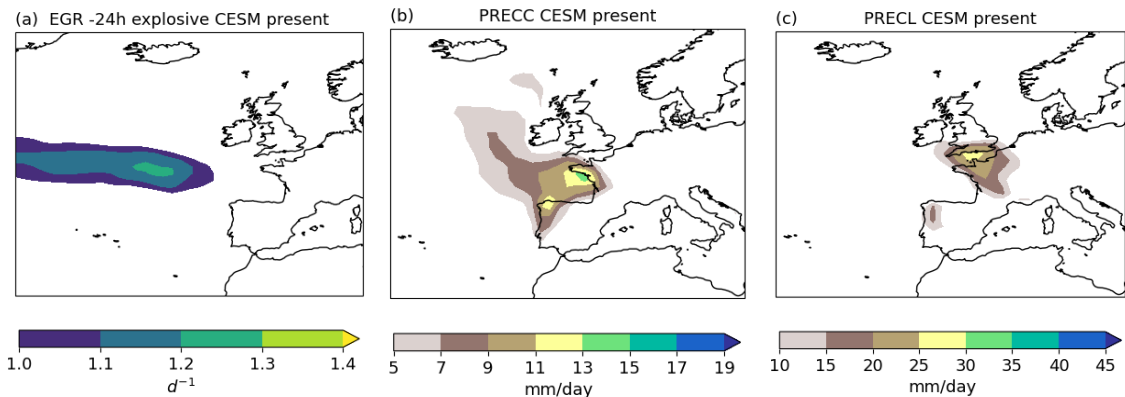
616 FIG. A1. 6-hourly tracks of storms Alex (a), Eunice (b), and Xynthia (c). (0) depicts the minimum sea level
617 pressure point, and (1) the position of the storm 24 hours before (0). The brown line indicates when the storm
618 underwent explosive cyclogenesis.

Alex			
Storm Angus	20 November 2016	United Kingdom, France	Also known as storm Nanette in France. The event left 2 fatalities and wind gusts up to 170 km/h (Sky News 2016; Met Office 2016; The telegraph 2016).
Storm Norberto	5 March 2020	France, Spain	Wind gusts around 100 km/h and up to 140 km/h were recorded (The European Forecaster 2021; AEMET 2021)
Storm Katie	28 March 2016	France, United Kingdom	The highest windgust recorded was 170 km/h in Isle of Wight (The European Forecaster 2021; AEMET 2021)
Eunice			
"Adolph Bermpohl" storm	23 February 1967	North Sea	The Adolph Bermpohl was a sea rescue cruiser on which its crew died due to the severity of the storm in the North Sea. Other boats also sank in the same storm (The Wreck Site 2017).
October storm	17 October 1967	Norway, Sweden	Hurricane-force winds of up to 144 km/h were recorded in some parts of southern Sweden (SMHI and Institute 2021).
Storm Capella	3 January 1976	Ireland, United Kingdom, Belgium, France, Denmark, Germany, Netherlands	Also known as Ruisbroek flood in Belgium. The storm resulted in severe wind damage across western and central Europe and coastal flooding. One of the strongest windgusts recorded during the event was 215 km/h at Lowther Hills (Met Office 1976). It left at least 82 fatalities (Berz 1988).
Burns' Day storm	25 January 1990	Ireland, United Kingdom, France, Belgium, Netherlands, Germany, Denmark	Also known as Storm Daria. Hurricane-force wind gust were recorded, such as 167 km/h at Abertporth (McCallum 1990) and 176 km/h at Pointe du Raz (Météo France 2019). The storm left at least 95 fatalities across Europe, being one of the deathliest storms in Europe (Météo France 2019).
Storm Oratia	30 October 2000	France, Germany, Netherlands and United Kingdom	Storm Oratia (Tora in Norway) (Extreme Wind Storms Catalogue n.d.) was probably the worst storm to hit United Kingdom after the Great Storm of 1987 (NASA Earth Observatory 2017). The storm brought heavy rainfall and strong winds to many areas of southern Britain, with wind gusts up to 150 km/h.
Storm Ulli	3 January 2012	United Kingdom, Ireland, Netherlands, Scandinavia	Storm Emil in Norway (The Nordic Page Norway n.d.). The damages were estimated at 0.2 billion USD (Koks and Haer 2020; Roberts et al. 2014b)
Storm Bronagh	21 September 2018	United Kingdom	Wind gusts up to 125 km/h recorded in the Isle of Wight (Met Office 2018).
Storm Christoph	21 January 2021	United Kingdom	The event was characterized by heavy precipitation above 100 mm. This was one of the wettest 3-day periods on record in the western and northwestern part of England and Wales (Met Office 2021).
Xynthia			
Storm Miguel	6 June 2019	Spain, France, Belgium, Luxembourg, Netherlands	The storm brought high winds and heavy precipitation to western Europe, with wind gusts up to 150 km/h (AEMET 2020; EUMETSAT 2019). It caused at least three deaths.

612 TABLE A1. Explosive analogues of each storm detected with ERA5, which are also known storms that had an
613 impact across Europe. The first column corresponds to the storm name, the second column shows the date of
614 minimum sea level pressure, the third column lists the regions affected, and the fourth column provides notes on
615 some meaningful aspects.



619 FIG. A2. Composites of the CESM present **analogues** and **explosive analogues** of **Alex** at their *time 0* dates
 620 of (a,d) sea-level pressure, (b,e) hourly mean precipitation rate, and (c,f) hourly mean wind speed.



621 FIG. A3. Composites of the CESM present **explosive analogues** of **Alex** at their *time 0* dates of (a) eady
 622 growth rate, (b) hourly mean convective precipitation, and (c) hourly mean large-scale precipitation rate.

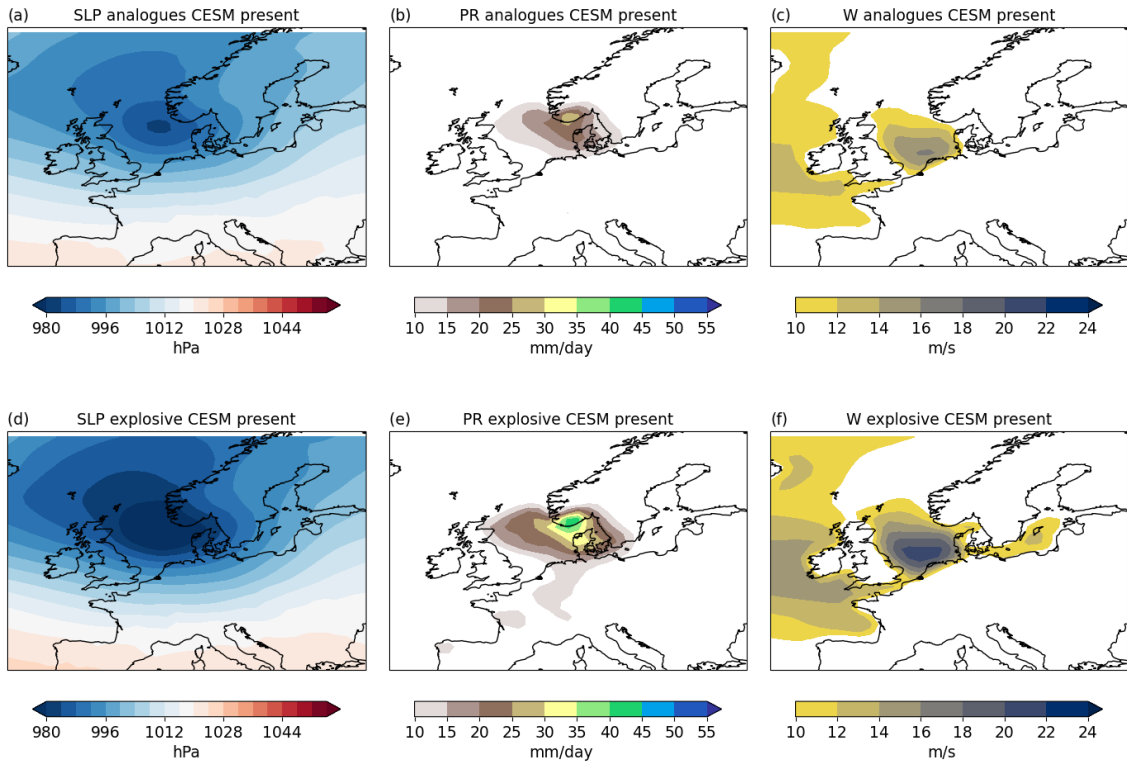


FIG. A4. Same than figure A2 but for **analogues of Eunice**.

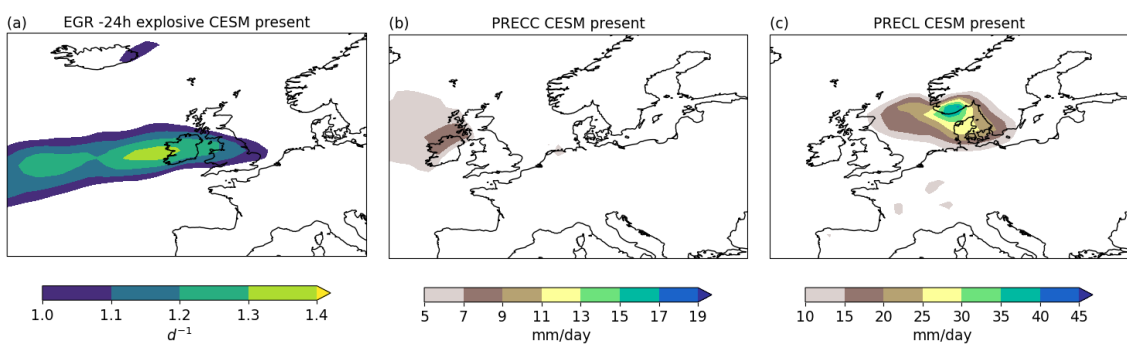


FIG. A5. Same than figure A3 but for **explosive analogues of Eunice**

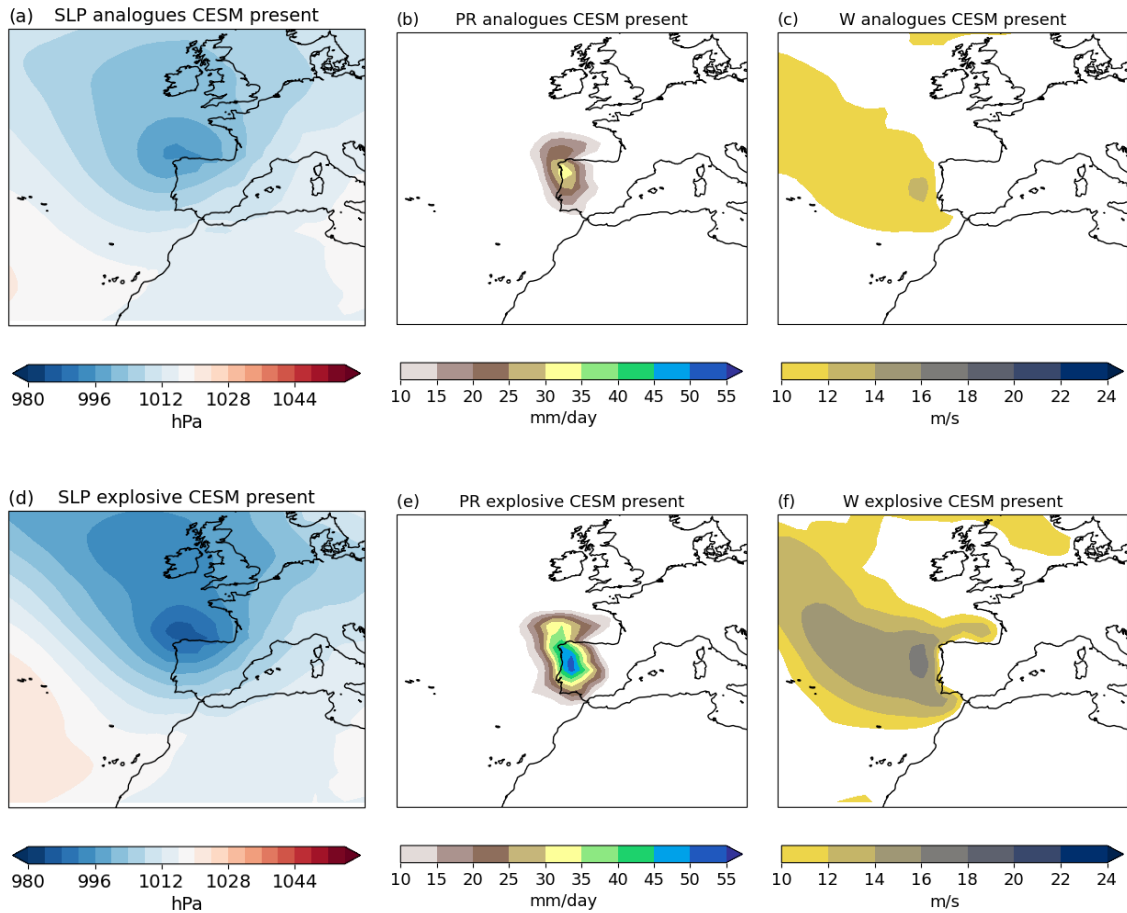


FIG. A6. Same than figure A2 but for **analogues of Xynthia**.

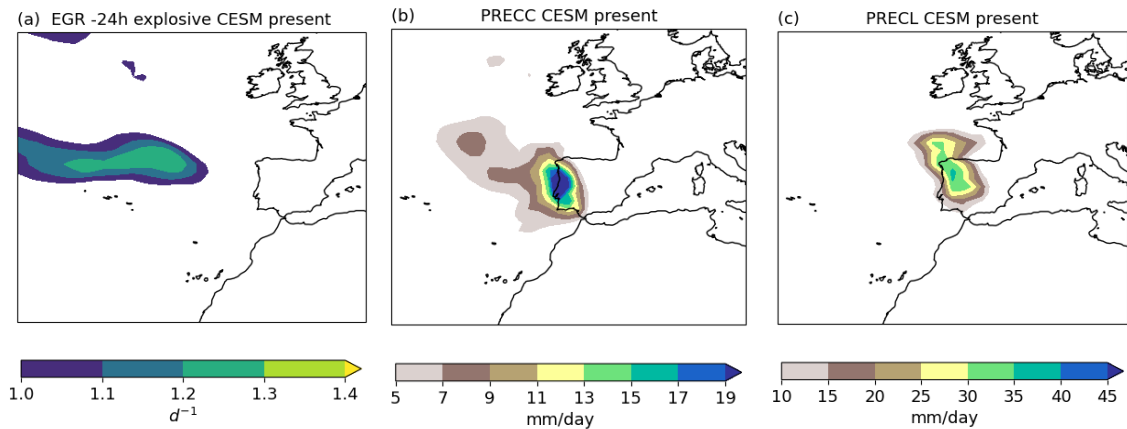


FIG. A7. Same than figure A3 but for **explosive analogues of Xynthia**

623 **References**

- 624 AEMET, 2020: Spanish state meteorological agency: Borrasca Miguel. Accessed: 2023-03-06,
625 https://www.aemet.es/ca/conocermas/borrascas/2018-2019/estudios_e_impactos/miguel.
- 626 AEMET, 2021: Spanish state meteorological agency: Borrasca Norberto. Accessed: 2023-03-06,
627 https://www.aemet.es/ca/conocermas/borrascas/2019-2020/estudios_e_impactos/norberto.
- 628 Anadolu Agency, 2022: Storm Eunice leaves 4 dead, over 400,000 homes
629 without power in Poland. Accessed: 2023-01-11, [https://www.aa.com.tr/en/europe/
630 storm-eunice-leaves-4-dead-over-400-000-homes-without-power-in-poland/2507945](https://www.aa.com.tr/en/europe/storm-eunice-leaves-4-dead-over-400-000-homes-without-power-in-poland/2507945).
- 631 Aon, 2020: Global Catastrophe Recap: October 2020. Available at: [http://thoughtleadership.aon.
632 com/documents/20201111_analytics-if-october-global-recap.pdf](http://thoughtleadership.aon.com/documents/20201111_analytics-if-october-global-recap.pdf) Accessed: October 2020.
- 633 BBC, 2022: Storm Eunice: Three people killed as strong winds sweep across UK. Accessed:
634 2023-01-11, <https://www.bbc.com/news/uk-60439651>.
- 635 Bertin, X., N. Bruneau, J.-F. Breilh, A. B. Fortunato, and M. Karpytchev, 2012: Importance of wave
636 age and resonance in storm surges: The case xynthia, bay of biscay. *Ocean Modelling*, **42**, 16–30,
637 <https://doi.org/https://doi.org/10.1016/j.ocemod.2011.11.001>, URL [https://www.sciencedirect.
638 com/science/article/pii/S1463500311001776](https://www.sciencedirect.com/science/article/pii/S1463500311001776).
- 639 Berz, G., 1988: List of major natural disasters, 1960–1987. *Natural Hazards*, **1 (1)**, 97–99.
- 640 Binder, H., H. Joos, M. Sprenger, and H. Wernli, 2023: Warm conveyor belts in present-day and fu-
641 ture climate simulations–part 2: Role of potential vorticity production for cyclone intensification.
642 *Weather and Climate Dynamics*, **4 (1)**, 19–37.
- 643 Brayshaw, D. J., B. Hoskins, , and M. Blackburn, 2009: The basic ingredients of the North
644 Atlantic storm track. Part I: Land–sea contrast and orography. *Journal of Atmospheric Sciences*,
645 **66**, 2539–2558, <https://doi.org/0.1175/2009JAS3078.1>.
- 646 Cattiaux, J., R. Vautard, C. Cassou, P. Yiou, V. Masson-Delmotte, and F. Codron, 2010: Winter
647 2010 in europe: A cold extreme in a warming climate. *Geophysical Research Letters*, **37 (20)**.
- 648 Catto, J. L., and Coauthors, 2019: The future of midlatitude cyclones. *Current Climate Change
649 Reports*, **5**, 407–420.

- 650 Chadenas, C., A. Creach, and D. Mercier, 2014: The impact of storm xynthia in 2010 on coastal
651 flood prevention policy in france. *Journal of Coastal Conservation*, **18 (5)**, 529–538.
- 652 Chauveau, E., and Coauthors, 2011: Xynthia: leçons d’une catastrophe. *Cybergeo: European*
653 *Journal of Geography*.
- 654 Clark, P. A., and S. L. Gray, 2018: Sting jets in extratropical cyclones: a review. *Quarterly*
655 *Journal of the Royal Meteorological Society*, **144 (713)**, 943–969, <https://doi.org/https://doi.org/10.1002/qj.3267>, URL <https://rmets.onlinelibrary.wiley.com/doi/abs/10.1002/qj.3267>, <https://rmets.onlinelibrary.wiley.com/doi/pdf/10.1002/qj.3267>.
- 658 Davolio, S., M. Vercellino, M. M. Miglietta, L. D. Pitura, S. Laviola, and V. Levizzani, 2022: The
659 influence of an atmospheric river on a heavy precipitation event over the western alps. *Weather*
660 *and Climate Extremes*, 100542.
- 661 Deser, C., A. Phillips, V. Bourdette, and H. Teng, 2012: Uncertainty in climate change projections:
662 the role of internal variability. *Climate dynamics*, **38 (3)**, 527–546.
- 663 Deutsche Welle, 2022: Europe reckons with cost of Storm Zeynep. Accessed: 2023-01-11, <https://www.dw.com/en/europe-reckons-with-cost-of-storm-zeynep/a-60823280>.
- 665 Dolores-Tesillos, E., F. Teubler, and S. Pfahl, 2022: Future changes in north atlantic winter cyclones
666 in cesm-le–part 1: Cyclone intensity, potential vorticity anomalies, and horizontal wind speed.
667 *Weather and Climate Dynamics*, **3 (2)**, 429–448.
- 668 EUMETSAT, 2019: Storm Miguel batters parts of Europe. Accessed: 2023-03-06, <https://www.eumetsat.int/storm-miguel-batters-parts-europe>.
- 670 European State of the Climate, 2020: Storm Alex. Accessed: 2023-03-06, <https://climate.copernicus.eu/esotc/2020/storm-alex>.
- 672 Extreme Wind Storms Catalogue, n.d.: Oratia (Tora). Accessed: 2023-03-06, http://www.europeanwindstorms.org/cgi-bin/storms/storms.cgi?storm1=Oratia_Tora.
- 674 Faranda, D., S. Bourdin, M. Ginesta, M. Krouma, G. Messori, R. Noyelle, F. Pons, and P. Yiou,
675 2022: A climate-change attribution retrospective of some impactful weather extremes of 2021.

- 676 Faranda, D., M. Ginesta, T. Alberti, E. Coppola, and M. Anzidei, 2023: Attributing venice acqua
677 alta events to a changing climate and evaluating the efficacy of mose adaptation strategy. *npj*
678 *Climate and Atmospheric Science*, **6** (1), 181.
- 679 Fink, A. H., T. Brücher, V. Ermert, A. Krüger, and J. G. Pinto, 2009: The european storm kyrill in
680 january 2007: synoptic evolution, meteorological impacts and some considerations with respect
681 to climate change. *Natural Hazards and Earth System Sciences*, **9** (2), 405–423, [https://doi.org/](https://doi.org/10.5194/nhess-9-405-2009)
682 10.5194/nhess-9-405-2009.
- 683 Fink, A. H., S. Pohle, J. G. Pinto, and P. Knippertz, 2012: Diagnosing the influence of diabatic
684 processes on the explosive deepening of extratropical cyclones. *Geophysical Research Letters*,
685 **39** (7).
- 686 Fischer, E. M., U. Beyerle, and R. Knutti, 2013: Robust spatially aggregated projections of climate
687 extremes. *Nature Climate Change*, **3** (12), 1033–1038.
- 688 García-Pereda (NWC SAF/AEMET), J., 2010: Storm Xynthia. URL [https://www.eumetsat.int/](https://www.eumetsat.int/storm-xynthia)
689 storm-xynthia.
- 690 Genovese, E., and V. Przyluski, 2013: Storm surge disaster risk management: the xynthia case
691 study in france. *Journal of Risk Research*, **16** (7), 825–841.
- 692 Ginesta, M., P. Yiou, G. Messori, and D. Faranda, 2022: A methodology for attributing severe
693 extratropical cyclones to climate change based on reanalysis data: the case study of storm alex
694 2020. *Climate Dynamics*, 1–25.
- 695 Harvey, B., P. Cook, L. Shaffrey, and R. Schiemann, 2020: The response of the northern hemisphere
696 storm tracks and jet streams to climate change in the cmip3, cmip5, and cmip6 climate models.
697 *Journal of Geophysical Research: Atmospheres*, **125** (23), e2020JD032 701.
- 698 Hawcroft, M., E. Walsh, K. Hodges, and G. Zappa, 2018: Significantly increased extreme
699 precipitation expected in europe and north america from extratropical cyclones. *Environ-*
700 *mental Research Letters*, **13** (12), 124 006, <https://doi.org/10.1088/1748-9326/aaed59>, URL
701 <https://doi.org/10.1088/1748-9326/aaed59>.
- 702 Hawcroft, M. K., L. C. Shaffrey, K. I. Hodges, and H. F. Dacre, 2012: How much northern
703 hemisphere precipitation is associated with extratropical cyclones? *Geophysical Research*

704 *Letters*, **39 (24)**, <https://doi.org/https://doi.org/10.1029/2012GL053866>, URL <https://agupubs.onlinelibrary.wiley.com/doi/abs/10.1029/2012GL053866>, <https://agupubs.onlinelibrary.wiley.com/doi/pdf/10.1029/2012GL053866>.

707 Hawkins, E., and R. Sutton, 2009: The potential to narrow uncertainty in regional climate predictions. *Bulletin of the American Meteorological Society*, **90 (8)**, 1095 – 1108, <https://doi.org/https://doi.org/10.1175/2009BAMS2607.1>, URL https://journals.ametsoc.org/view/journals/bams/90/8/2009bams2607_1.xml.

711 Hersbach, H., and Coauthors, 2020: The era5 global reanalysis. *Quarterly Journal of the Royal Meteorological Society*, **146 (730)**, 1999–2049, <https://doi.org/https://doi.org/10.1002/qj.3803>, URL <https://rmets.onlinelibrary.wiley.com/doi/abs/10.1002/qj.3803>, <https://rmets.onlinelibrary.wiley.com/doi/pdf/10.1002/qj.3803>.

715 Hurrell, J. W., and Coauthors, 2013: The community earth system model: a framework for collaborative research. *Bulletin of the American Meteorological Society*, **94 (9)**, 1339–1360.

717 Jansa, A., P. Alpert, A. Buzzi, and P. Arbogast, 2001: Medex, cyclones that produce high impact weather in the mediterranean. *Avalaible at http://medex.aemet.uib.es*.

719 Jézéquel, A., V. Dépoues, H. Guillemot, M. Trolliet, J.-P. Vanderlinden, and P. Yiou, 2018: Behind the veil of extreme event attribution. *Climatic Change*, **149**, 367–383.

721 Joos, H., M. Sprenger, H. Binder, U. Beyerle, and H. Wernli, 2023: Warm conveyor belts in present-day and future climate simulations-part 1: Climatology and impacts. *Weather and Climate Dynamics*, **4 (1)**, 133–155.

724 Kay, J. E., and Coauthors, 2015: The community earth system model (cesm) large ensemble project: A community resource for studying climate change in the presence of internal climate variability. *Bulletin of the American Meteorological Society*, **96 (8)**, 1333–1349.

727 Koks, E., and T. Haer, 2020: A high-resolution wind damage model for europe. *Scientific Reports*, **10**, 6866, <https://doi.org/10.1038/s41598-020-63580-w>.

729 Kolen, B., R. Slomp, and S. Jonkman, 2013: The impacts of storm xynthia february 27–28, 2010 in france: lessons for flood risk management. *Journal of Flood Risk Management*, **6 (3)**, 261–278,

730

- 731 <https://doi.org/https://doi.org/10.1111/jfr3.12011>, URL [https://onlinelibrary.wiley.com/doi/abs/](https://onlinelibrary.wiley.com/doi/abs/10.1111/jfr3.12011)
732 [10.1111/jfr3.12011](https://onlinelibrary.wiley.com/doi/pdf/10.1111/jfr3.12011), <https://onlinelibrary.wiley.com/doi/pdf/10.1111/jfr3.12011>.
- 733 Lehmann, J., D. Coumou, K. Frieler, A. V. Eliseev, and A. Levermann, 2014: Future changes
734 in extratropical storm tracks and baroclinicity under climate change. *Environmental Research*
735 *Letters*, **9 (8)**, 084 002.
- 736 Liberato, M., J. Pinto, R. Trigo, P. Ludwig, P. Ordóñez, D. Yuen, and I. Trigo, 2013: Explosive
737 development of winter storm xynthia over the subtropical north atlantic ocean. *Natural Hazards*
738 *and Earth System Sciences*, **13 (9)**, 2239–2251.
- 739 Liberato, M. L., 2014: The 19 january 2013 windstorm over the north atlantic: large-scale
740 dynamics and impacts on iberia. *Weather and Climate Extremes*, **5-6**, 16–28, <https://doi.org/https://doi.org/10.1016/j.wace.2014.06.002>, URL [https://www.sciencedirect.com/science/article/pii/](https://www.sciencedirect.com/science/article/pii/S2212094714000620)
741 [S2212094714000620](https://www.sciencedirect.com/science/article/pii/S2212094714000620).
742
- 743 Liu, W. T., W. Tang, and X. Xie, 2008: Wind power distribution over the ocean. *Geophys-*
744 *ical Research Letters*, **35 (13)**, <https://doi.org/https://doi.org/10.1029/2008GL034172>,
745 URL <https://agupubs.onlinelibrary.wiley.com/doi/abs/10.1029/2008GL034172>, <https://agupubs.onlinelibrary.wiley.com/doi/pdf/10.1029/2008GL034172>.
746
- 747 Ludwig, P., J. G. Pinto, M. Reyers, and S. L. Gray, 2014: The role of anomalous sst and surface
748 fluxes over the southeastern north atlantic in the explosive development of windstorm xynthia.
749 *Quarterly Journal of the Royal Meteorological Society*, **140 (682)**, 1729–1741.
- 750 Manning, C., E. J. Kendon, H. J. Fowler, N. M. Roberts, S. Berthou, D. Suri, and M. J. Roberts,
751 2022: Extreme windstorms and sting jets in convection-permitting climate simulations over
752 europe. *Climate Dynamics*, **58 (9)**, 2387–2404.
- 753 Massacand, A. C., H. Wernli, and H. C. Davies, 1998: Heavy precipitation on the alpine southside:
754 An upper-level precursor. *Geophysical Research Letters*, **25 (9)**, 1435–1438, [https://doi.org/](https://doi.org/https://doi.org/10.1029/98GL50869)
755 <https://doi.org/10.1029/98GL50869>, URL [https://agupubs.onlinelibrary.wiley.com/doi/abs/10.](https://agupubs.onlinelibrary.wiley.com/doi/abs/10.1029/98GL50869)
756 [1029/98GL50869](https://agupubs.onlinelibrary.wiley.com/doi/pdf/10.1029/98GL50869), <https://agupubs.onlinelibrary.wiley.com/doi/pdf/10.1029/98GL50869>.
- 757 McCallum, E., 1990: The burns' day storm, 25 january 1990. *Weather*, **45 (5)**, 166–173.

758 Meinshausen, M., and Coauthors, 2011: The rcp greenhouse gas concentrations and their exten-
759 sions from 1765 to 2300. *Climatic change*, **109** (1), 213–241.

760 Met Office, 1976: Monthly weather report: January 1976. Available at [https://web.archive.org/
761 web/20121023103203/http://www.metoffice.gov.uk/media/pdf/m/r/Jan1976.pdf](https://web.archive.org/web/20121023103203/http://www.metoffice.gov.uk/media/pdf/m/r/Jan1976.pdf).

762 Met Office, 2016: Storm angus. Available at [https://www.metoffice.gov.uk/weather/
763 warnings-and-advice/uk-storm-centre/storm-angus](https://www.metoffice.gov.uk/weather/warnings-and-advice/uk-storm-centre/storm-angus).

764 Met Office, 2018: Storm bronagh. Accessed: 2023-03-06, [https://www.metoffice.gov.uk/weather/
765 warnings-and-advice/uk-storm-centre/storm-bronagh](https://www.metoffice.gov.uk/weather/warnings-and-advice/uk-storm-centre/storm-bronagh).

766 Met Office, 2021: Storm Christoph 18 to 20 January 2021. Accessed: 2023-03-06,
767 [https://www.metoffice.gov.uk/binaries/content/assets/metofficegovuk/pdf/weather/learn-about/
768 uk-past-events/interesting/2021/2021_01_storm_christoph.pdf](https://www.metoffice.gov.uk/binaries/content/assets/metofficegovuk/pdf/weather/learn-about/uk-past-events/interesting/2021/2021_01_storm_christoph.pdf).

769 Met Office, 2022: Storms dudley, eunice and franklin, february 2022. Available at:
770 [https://www.metoffice.gov.uk/binaries/content/assets/metofficegovuk/pdf/weather/learn-about/
771 uk-past-events/interesting/2022/2022_01_storms_dudley_eunice_franklin.r1.pdf](https://www.metoffice.gov.uk/binaries/content/assets/metofficegovuk/pdf/weather/learn-about/uk-past-events/interesting/2022/2022_01_storms_dudley_eunice_franklin.r1.pdf) Accessed:
772 March 2023.

773 Michaelis, A. C., J. Willison, G. M. Lackmann, and W. A. Robinson, 2017: Changes
774 in winter north atlantic extratropical cyclones in high-resolution regional pseudo–global
775 warming simulations. *Journal of Climate*, **30** (17), 6905 – 6925, [https://doi.org/https:
776 //doi.org/10.1175/JCLI-D-16-0697.1](https://doi.org/https://doi.org/10.1175/JCLI-D-16-0697.1), URL [https://journals.ametsoc.org/view/journals/clim/30/
777 17/jcli-d-16-0697.1.xml](https://journals.ametsoc.org/view/journals/clim/30/17/jcli-d-16-0697.1.xml).

778 Météo France, 2019: Tempête DARIA du 25 janvier 1990. Available at [http://tempetes.meteo.fr/
779 IMG/anthemis_pdf/19900125.pdf](http://tempetes.meteo.fr/IMG/anthemis_pdf/19900125.pdf).

780 Météo France, 2020: Tempête Alex: des intempéries exceptionnelles. Available at [https://
781 meteofrance.com/actualites-et-dossiers/climat/tempete-alex-des-intemperies-exceptionnelles](https://meteofrance.com/actualites-et-dossiers/climat/tempete-alex-des-intemperies-exceptionnelles).

782 NASA Earth Observatory, 2017: Superstorm Sweeps Over England. Accessed: 2023-03-06,
783 <https://wrecksite.eu/wreck.aspx?258019>.

- 784 Neu, U., and Coauthors, 2013: Imilast: A community effort to intercompare extratropical cyclone
785 detection and tracking algorithms. *Bulletin of the American Meteorological Society*, **94** (4),
786 529–547.
- 787 NL Times, 2022: Fourth death confirmed in Netherlands as Storm Eunice heads north. Accessed: 2023-01-11, [https://nltimes.nl/2022/02/18/
788 fourth-death-confirmed-netherlands-storm-eunice-heads-north.](https://nltimes.nl/2022/02/18/fourth-death-confirmed-netherlands-storm-eunice-heads-north)
- 790 Owen, L. E., J. L. Catto, D. B. Stephenson, and N. J. Dunstone, 2021: Compound precipitation and
791 wind extremes over Europe and their relationship to extratropical cyclones. *Weather and Climate
792 Extremes*, **33**, 100342, [https://doi.org/https://doi.org/10.1016/j.wace.2021.100342](https://doi.org/10.1016/j.wace.2021.100342), URL <https://www.sciencedirect.com/science/article/pii/S2212094721000384>.
- 794 Priestley, M. D. K., D. Ackerley, J. L. Catto, K. I. Hodges, R. E. McDonald, and R. W. Lee, 2020:
795 An overview of the extratropical storm tracks in cmip6 historical simulations. *Journal of Climate*,
796 **33** (15), 6315 – 6343, <https://doi.org/10.1175/JCLI-D-19-0928.1>, URL [https://journals.ametsoc.
797 org/view/journals/clim/33/15/JCLI-D-19-0928.1.xml](https://journals.ametsoc.org/view/journals/clim/33/15/JCLI-D-19-0928.1.xml).
- 798 Priestley, M. D. K., and J. L. Catto, 2022: Future changes in the extratropical storm tracks and
799 cyclone intensity, wind speed, and structure. *Weather and Climate Dynamics*, **3** (1), 337–360,
800 <https://doi.org/10.5194/wcd-3-337-2022>, URL <https://wcd.copernicus.org/articles/3/337/2022/>.
- 801 Rapella, L., D. Faranda, M. Gaetani, D. Philippe, and M. Ginesta, 2023: Climate change on extreme
802 winds already affects off-shore wind power availability in Europe. *Environmental Research
803 Letters*.
- 804 Reale, M., M. L. Liberato, P. Lionello, J. G. Pinto, S. Salon, and S. Ulbrich, 2019: A global clima-
805 tology of explosive cyclones using a multi-tracking approach. *Tellus A: Dynamic Meteorology
806 and Oceanography*, **71** (1), 1611–1634, <https://doi.org/10.1080/16000870.2019.1611340>.
- 807 RMS, 2022: RMS estimates insured losses from windstorms Dudley and Eunice
808 will likely range between 3.0 and 4.5 billion euro. Accessed: 2023-
809 01-11, [https://www.rms.com/newsroom/press-releases/press-detail/2022-03-01/
810 rms-estimates-insured-losses-from-windstorms-dudley-and-eunice-will-likely-range-between-30-and-45](https://www.rms.com/newsroom/press-releases/press-detail/2022-03-01/rms-estimates-insured-losses-from-windstorms-dudley-and-eunice-will-likely-range-between-30-and-45)

- 811 Roberts, J., and Coauthors, 2014a: The xws open access catalogue of extreme european windstorms
812 from 1979 to 2012. *Natural Hazards and Earth System Sciences*, **14** (9), 2487–2501.
- 813 Roberts, J. F., and Coauthors, 2014b: The xws open access catalogue of extreme european
814 windstorms from 1979 to 2012. *Natural Hazards and Earth System Sciences*, **14** (9), 2487–
815 2501, <https://doi.org/10.5194/nhess-14-2487-2014>, URL [https://nhess.copernicus.org/articles/
816 14/2487/2014/](https://nhess.copernicus.org/articles/14/2487/2014/).
- 817 Roebber, P. J., 1984: Statistical analysis and updated climatology of explosive cyclones. *Monthly*
818 *Weather Review*, **112**, 1577–1589, [https://doi.org/https://doi.org/10.1175/1520-0493\(1984\)
819 112\(1577:SAAUCO\)2.0.CO;2](https://doi.org/https://doi.org/10.1175/1520-0493(1984)112(1577:SAAUCO)2.0.CO;2).
- 820 Röthlisberger, M., M. Sprenger, E. Flaounas, U. Beyerle, and H. Wernli, 2020: The substructure of
821 extremely hot summers in the northern hemisphere. *Weather and Climate Dynamics*, **1** (1), 45–62,
822 <https://doi.org/10.5194/wcd-1-45-2020>, URL <https://wcd.copernicus.org/articles/1/45/2020/>.
- 823 RTL Info, 2022: La tempête Eunice a balayé la Belgique: le bilan s'alourdit à 2 morts, les pompiers
824 surchargés un peu partout dans le pays. Accessed: 2023-01-11, [https://www.rtl.be/info/belgique/
825 meteo/meteo-un-vent-tempetueux-attendu-ce-vendredi-voici-les-previsions-1357970.aspx](https://www.rtl.be/info/belgique/meteo/meteo-un-vent-tempetueux-attendu-ce-vendredi-voici-les-previsions-1357970.aspx).
- 826 Sanders, F., and J. R. Gyakum, 1980: Synoptic-dynamic climatology of the “bomb”. *Monthly*
827 *Weather Review*, **108**, 1589–1606, [https://doi.org/https://doi.org/10.1175/1520-0493\(1980\)
828 108\(1589:SDCOT\)2.0.CO;2](https://doi.org/https://doi.org/10.1175/1520-0493(1980)108(1589:SDCOT)2.0.CO;2).
- 829 Sansom, P. G., D. B. Stephenson, C. A. Ferro, G. Zappa, and L. Shaffrey, 2013: Simple uncertainty
830 frameworks for selecting weighting schemes and interpreting multimodel ensemble climate
831 change experiments. *Journal of Climate*, **26** (12), 4017–4037.
- 832 Schemm, S., 2023: Toward eliminating the decades-old “too zonal and too equatorward”
833 storm-track bias in climate models. *Journal of Advances in Modeling Earth Systems*,
834 **15** (2), e2022MS003482, <https://doi.org/https://doi.org/10.1029/2022MS003482>, URL
835 <https://agupubs.onlinelibrary.wiley.com/doi/abs/10.1029/2022MS003482>, e2022MS003482
836 2022MS003482, <https://agupubs.onlinelibrary.wiley.com/doi/pdf/10.1029/2022MS003482>.
- 837 Seiler, C., and F. W. Zwiers, 2016: How will climate change affect explosive cyclones in the
838 extratropics of the northern hemisphere? *Climate Dynamics*, **46** (11), 3633–3644.

839 Seneviratne, S., and Coauthors, 2021: Weather and climate extreme events in a changing climate. In
840 Climate Change 2021: The physical science basis. Contribution of Working Group I to the Sixth
841 Assessment Report of the Intergovernmental Panel on Climate Change [Masson-Delmotte, V.,
842 P. Zhai, A. Pirani, S.L. Connors, C. Péan, S. Berger, N. Caud, Y. Chen, L. Goldfarb, M.I. Gomis,
843 M. Huang, K. Leitzell, E. Lonnoy, J.B.R. Matthews, T.K. Maycock, T. Waterfield, O. Yelekçi,
844 R. Yu, and B. Zhou (eds.)]. Cambridge University Press. In Press. Cambridge University Press.

845 Shapiro, M. A., and D. Keyser, 1990: *Fronts, Jet Streams and the Tropopause*, 167–191. American
846 Meteorological Society, Boston, MA, https://doi.org/10.1007/978-1-944970-33-8_10, URL
847 https://doi.org/10.1007/978-1-944970-33-8_10.

848 Shaw, T. A., and Coauthors, 2016: Storm track processes and the opposing influences of climate
849 change. *Nature Geosci*, **9**, 656–664, <https://doi.org/https://doi.org/10.1038/ngeo2783>.

850 Shepherd, T. G., 2016: A common framework for approaches to extreme event attribution. *Current*
851 *Climate Change Reports*, **2**, 28–38.

852 Sinclair, V. A., M. Rantanen, P. Haapanala, J. Räisänen, and H. Järvinen, 2020: The characteristics
853 and structure of extra-tropical cyclones in a warmer climate. *Weather and Climate Dynamics*,
854 **1** (1), 1–25, <https://doi.org/10.5194/wcd-1-1-2020>, URL [https://wcd.copernicus.org/articles/1/](https://wcd.copernicus.org/articles/1/1/2020/)
855 [1/2020/](https://wcd.copernicus.org/articles/1/1/2020/).

856 Sky News, 2016: Storm angus: Body found in search for pensioner after flood. Available at
857 <https://news.sky.com/story/woman-dies-after-folkestone-storm-angus-rescue-10667386>.

858 SMHI, S. M., and H. Institute, 2021: Den svåra oktoberstormen 1967. Ac-
859 cessed: 2023-03-06, [https://www.smhi.se/kunskapsbanken/meteorologi/stormar-i-sverige/](https://www.smhi.se/kunskapsbanken/meteorologi/stormar-i-sverige/enskilda-stormar-och-ovader/den-svara-oktoberstormen-1967-1.5744)
860 [enskilda-stormar-och-ovader/den-svara-oktoberstormen-1967-1.5744](https://www.smhi.se/kunskapsbanken/meteorologi/stormar-i-sverige/enskilda-stormar-och-ovader/den-svara-oktoberstormen-1967-1.5744).

861 The European Forecaster, 2021: The European Forecaster Newsletter of the WGCEF N° 26
862 September 2021. Accessed: 2023-03-06, <http://www.euroforecaster.org/newsletter26/full.pdf>.

863 The Irish Times, 2022: Storm Eunice: Council worker dies in Wexford after being struck
864 by falling tree. Accessed: 2023-01-11, [https://www.irishtimes.com/news/ireland/irish-news/](https://www.irishtimes.com/news/ireland/irish-news/storm-eunice-council-worker-dies-in-wexford-after-being-struck-by-falling-tree-1.4805979)
865 [storm-eunice-council-worker-dies-in-wexford-after-being-struck-by-falling-tree-1.4805979](https://www.irishtimes.com/news/ireland/irish-news/storm-eunice-council-worker-dies-in-wexford-after-being-struck-by-falling-tree-1.4805979).

866 The Nordic Page Norway, n.d.: “Emil” to hit southern Norway. Available at <https://www.tnp.no/norway/panorama/2601-34emil34-is-to-strike-southern-norway/>.

867

868 The telegraph, 2016: UK weather: Woman dies after being winched from the sea
869 as storm Angus batters Britain. Available at [https://www.telegraph.co.uk/news/2016/11/21/
870 uk-weather-heavy-rain-causes-flooding-wake-storm-angus/](https://www.telegraph.co.uk/news/2016/11/21/uk-weather-heavy-rain-causes-flooding-wake-storm-angus/).

871 The Wreck Site, 2017: MV Adolph Bermpohl (+1967) . Accessed: 2023-03-06, [https://wrecksite.
872 eu/wreck.aspx?258019](https://wrecksite.eu/wreck.aspx?258019).

873 Trenberth, K. E., J. T. Fasullo, and T. G. Shepherd, 2015: Attribution of climate extreme events.
874 *Nature Climate Change*, **5 (8)**, 725–730.

875 Uccellini, L. W., 1990: Processes contributing to the rapid development of extratropical cyclones.
876 *Extratropical Cyclones: The Erik Palmén Memorial Volume*, 81–105.

877 Vinet, F., D. Lumbroso, S. Defossez, and L. Boissier, 2012: A comparative analysis of the loss of
878 life during two recent floods in France: the sea surge caused by the storm Xynthia and the flash
879 flood in Var. *Natural Hazards*, **61 (3)**, 1179–1201.

880 Wallace, J. M., and P. V. Hobbs, 2006: 10 - climate dynamics. *Atmospheric Science (Second
881 Edition)*, J. M. Wallace, and P. V. Hobbs, Eds., second edition ed., Academic Press, San
882 Diego, 419–465, <https://doi.org/https://doi.org/10.1016/B978-0-12-732951-2.50015-6>, URL
883 <https://www.sciencedirect.com/science/article/pii/B9780127329512500156>.

884 Wernli, H., and C. Schwierz, 2006: Surface cyclones in the ERA-40 dataset (1958–2001). part
885 i: Novel identification method and global climatology. *Journal of the Atmospheric Sciences*,
886 **63 (10)**, 2486–2507.

887 WMO, 2020: Mediterranean episode causes “unprecedented” rainfall. Available at [https://public.
888 wmo.int/en/media/news/mediterranean-episode-causes-unprecedented-rainfall](https://public.wmo.int/en/media/news/mediterranean-episode-causes-unprecedented-rainfall).

889 Worlwide, A., 2010: European Winterstorm Xynthia. URL [https://alert.air-worldwide.com/
890 extratropical-cyclone/2010/european-winterstorm-xynthia/update-1/](https://alert.air-worldwide.com/extratropical-cyclone/2010/european-winterstorm-xynthia/update-1/).

891 Yiou, P., 2014: Anawege: a weather generator based on analogues of atmospheric circulation.
892 *Geoscientific Model Development*, **7 (2)**, 531–543.

893 Zappa, G., L. Shaffrey, K. Hodges, P. Sansom, and D. Stephenson, 2013: A multimodel assessment
894 of future projections of north atlantic and european extratropical cyclones in the cmip5 climate
895 models. *Journal of Climate*, **26**, 5846–5862, <https://doi.org/10.1175/JCLI-D-12-00573.1>.

896 Zhang, Z., and B. A. Colle, 2017: Changes in extratropical cyclone precipitation and associated
897 processes during the twenty-first century over eastern north america and the western atlantic
898 using a cyclone-relative approach. *Journal of Climate*, **30** (21), 8633 – 8656, <https://doi.org/https://doi.org/10.1175/JCLI-D-16-0906.1>, URL <https://journals.ametsoc.org/view/journals/clim/30/21/jcli-d-16-0906.1.xml>.
899
900